DNA/Ca –Adsorption an Lipidmembran-Oberflächen für den effizienten elektroporativen Gen-Transfer in Gewebezellen

Dissertation

zur Erlangung des

Doktorgrades der Naturwissenschaften

an der Universität Bielefeld

von

Alina Frantescu

Bielefeld, April 2005

Inhaltsverzeichnis

Zusammenfassung

Der elektroporative Transfer von DNA und anderen bioaktiven Substanzen durch Zellmembranen mittels elektrischer Pulse gewinnt zunehmend an Bedeutung in den neuen Disziplinen der Elektrochemotherapie und Elektrogentherapie. Die Effektivität des Elektrotransfers hängt wesentlich von der Adsorption der Gen-DNA und der Oligonucleotide an die Plasmazellmembran ab. Hier wird gezeigt, dass die Adsorption von längeren Oligonucleotiden, wie zum Beispiel ultraschall-behandelte Kalbs-Thymus DNA-Fragmente im Größenbereich von zirka 300 Basenparen an Lipidvesikel mit einem Durchmesser von Φ = 300 ± 90 nm durch divalente Kationen, wie z.B. Ca^{2+} -Ionen, wesentlich verstärkt ist. Durch Zentrifugation werden freie und gebundene DNA bei der Wellenlänge λ = 260 nm optisch bestimmt. Mittels Atom-Absorptionsspektrometrie (AAS) und mit Hilfe des Ca^{2+}-Indikators Arsenazo-III werden die Dissoziationsgleichgewichtskonstanten sowohl der individuellen Binärkomplexe von Ca^{2+} und DNA-Bindung: Ca^{2+}/Vesikel, DNA/Vesikel und Ca^{2+}/DNA als auch die der drei verschiedenen Prozesse bestimmt, die zu dem Ternärkomplex: Ca^{2+}/DNA/Vesikel führen.

Die Turbiditätsrelaxationen der Vesikelsuspension bei der Wellenlänge λ = 365 nm in äußeren elektrischen Feldern mit Feldstärken von E / (kV/cm) = 30 und 40 und der Pulsdauer t_E = 10 μs deuten an, dass die Elektroelongationen der Vesikel mit der Glättung der thermischen Ondulationen, Ausdehnung der Membran und bei höheren Feldstärken E ≥ 40 kV/cm, auch mit der Elektroporation gekoppelt sind. Die quantitative Analyse der Ausdehnungskinetik zeigt, dass die DNA Adsorption an die Vesikeloberfläche als Ternärkomplex DNA/Ca/Lipide die Membran weicher macht und damit die Elektroporation erleichtert. Beispielsweise, bei E = 30 kV/cm und $[Ca_t]$ = 0,25 mM bewirken die membrangebundenen DNA-Fragmente im Konzentrationsbereich $0 \le [D_b]/\mu M(bp) \le 40$, d. h. $0 \le N_b \le 118$ DNA-Fragmente je Vesikel, dass sowohl die Biegesteifigkeit im Bereich $17 \ge \kappa/(10^{-20} J) \ge 13$ als auch der Ausdehnungsmodul im Bereich $1,2 \ge K/(N/m) \ge 0,83$ reduziert werden.

Mit der Kenntnis aller Gleichgewichtskonstanten der Teilreaktionen der Entstehung des Ternärkomplexes und dem Verhalten des Ternärkomplexes DNA/Ca/Lipidvesikel in äußeren elektrischen Feldern, kann man nun zielgerichtet die DNA-Adsorption für den elektroporativen Gentransfer, auch in der Elektrogentherapie, optimieren.

Die vorliegende Dissertation ist in drei Teile gegliedert: die deutsch geschriebene Einleitung (I) und zwei Publikationsentwürfe (II) und (III).

I. Einleitung

II. ″Interfacial ternary complex DNA/Ca/Lipids at anionic vesicle surfaces″, submitted to Bioelectrochemistry

III. ″Adsorption of DNA and electric fields decrease the rigidity of lipid vesicle membranes″, submitted to Physical Chemistry Chemical Physics (PCCP)

DNA/Ca –Adsorption an Lipidmembran-Oberflächen für den effizienten elektroporativen Gen-Transfer in Gewebezellen

I. Einleitung

In der Elektochemotherapie und der Elektrogentherapie ist der Elektrotransfer von DNA und anderen bioaktiven Substanzen durch die Zellmembranen, insbesondere von Gewebezellen, von erheblicher biotechnologischer Bedeutung [II, ref. 1]. Der Begriff und die Technik der Membranelektroporation (ME) für Gen-Elektrotransfer wurden bereits 1982 eingeführt [II, ref. 2]. Die ME ist eine Gentranfer-Alternative zu den viralen Genen, aber ohne die bekannten Nebenwirkungen [II, refs. 1, 3, 4]. Die Wirksamkeit des Elektrotransfers mit ″nackten″ Oligo- [II, ref. 5] und Polynucleotiden bei moderaten, harmlosen elektrischen Feldpulsen, kann deutlich verbessert werden, wenn die Gen-DNA, vor Anlegen der therapeutischen Hochfeldpulse, an die Zelloberflächen adsorbiert ist.

Die gekrümmten Lipidvesikeloberflächen dienen als Modell für den Lipidteil der zellulären Membranoberflächen [III, refs. 8, 9]. Die Mehrzahl aller Zellmembranen ist durch anionische Lipide negativ geladen. Um nun die Adsorption von negativ geladenen Polyelektrolyten wie DNA an Zelloberflächen zu erhöhen, werden entweder Ca^{2+} oder Mg^{2+} -Ionen als ″verbrückende″ Ionen eingesetzt [II, refs. 2, 15, 16]. In dieser Arbeit wird die DNA-Adsorption an anionische Lipidvesikeloberflächen als Modell für den Lipidteil der Zellmembranen aus anionischen (bei pH 7,4) Lipidmischungen quantifiziert. Ca^{2+}-Ionen werden als ″elektrostatische Brücke″ verwendet, um DNA an die Vesikeloberfläche zu binden.

Die Wechselwirkung zwischen Ca^{2+} - Ionen und Lipidvesikeln aus unterschiedlichen Lipiden ist bereits untersucht worden [II, refs. 6-9]. Auch die Bindung von DNA an positiv geladene Vesikeloberflächen wurde quantifiziert [III, refs. 17-21] und auch die Wechselwirkung zwischen DNA und verschiedenen mono- und divalenten Kationen wurde beschrieben [II, refs. 12-14].

Im ersten Teil dieser Arbeit wird zunächst das Problem der Ternärkomplexe im allgemeinen abgehandelt, um dann die Prozesse zu analysieren, die zum Ternärkomplex DNA/Ca/Lipidvesikel führen. Die Entstehung des Ternärkomplexes DNA/Ca/Lipide wurde auch an Lipidmonoschichten beobachtet [II, ref. 17]. Durch Zentrifugation des Vesikelanteils, optische Indikation und Atomabsorptionsspektrometrie (AAS) des Überstandes werden die Dissoziationsgleichgewichtkonstanten sowohl der Binärkomplexe: Ca^{2+}/Vesikel, DNA/Vesikel und Ca^{2+}/DNA, als auch aller Ternärkomplex-Bildungsprozesse bestimmt, die zur Spezies Ca^{2+}/DNA/Vesikel führen.

Im zweiten Teil dieser Arbeit wird das Verhalten der Lipidvesikel bei Anlegen von Rechteckpulsen mit Feldstärken von E / (kV/cm) = 30 und 40 und der Dauer t_E = 10 µs untersucht. Es ist bekannt, dass in elektrischen Feldern die fast ″kugelförmigen″ Lipidvesikel in ein Rotationsellipsoid mit der langen Halbachse in Richtung des Feldes elongiert werden [III, ref. 27]. Die feld-induzierte Dehnung der Membran führt bei konstantem Volumen zum Anstieg der Membranoberfläche und bedingt bei höheren Feldstärken E ≥ 40 kV/cm weiteres Eindringen von Wasser in die Membran, dass zur Porenbildung führt [III, refs. 26, 27].

Die elastischen Eigenschaften der Lipidmembran, charakterisiert durch den Ausdehnungsmodul K und die Biegesteifigkeit κ bestimmen auch die Wechselwirkungen zwischen den kolloidalen Nanopartikeln und Polymeren mit positiv geladenen Vesikeln [III, refs. 11-13]. Es ist bekannt, dass die Änderung der elastischen Eigenschaften der Membranen durch adsorbierte und insertierte Polymere einerseits und durch äußere elektrische Felder andererseits geändert werden können [III, refs. 12, 14, 15]. Die Komplexbildung von DNA und kationischen Vesikeloberflächen kann zu multilamellaren Partikeln führen. Bei höheren DNA Konzentrationen kann es zur Auflösung von Vesikeln und der Bildung von multilamellaren Lipidkomplexen kommen [III, refs. 23, 24]. Um Aggregationen zu vermeiden, werden hier kleinere unilamellare anionische Vesikel, geringe Lipid [L_t] und Ca^{2+} - Ionen [Ca_t] Konzentrationen verwendet [III, ref. 25].

Die elektrischen Pulse führen zur Glättung der Membranondulationen, Ausdehnung der Membran und bei höheren Feldstärken E ≥ 40 kV/cm, zur Elektroporation. Die dadurch bewirkte Membranoberflächenvergrößerung führt letztendlich zur weiteren Vesikelelongation [III, ref. 26]. Hier wird die Wirkung der DNA-Adsorption an die Membraneoberflächen auf die Kinetik der Vesikelelongationen in elektrischen Feldern analysiert und der Feldstärke-bereich ermittelt, oberhalb dessen die elektrische Porenbildung den Durchtritt der DNA-Fragmente verstärken kann.

II. Eingereichtes Manuskript: submittet to Bioelectrochemistry

Interfacial ternary complex DNA/Ca/Lipids at anionic vesicle surfaces

Alina Frantescu, Katja Tönsing and Eberhard Neumann*

Physical and Biophysical Chemistry, Faculty of Chemistry, University of Bielefeld, P. O. Box 100131, D-33615 Bielefeld, Germany.

Key words: polynucleotides, oligonucleotides, Ca-binding constants, electrified membrane interface, monolayer adsorption, complex thermodynamics

*Correspondence to: Prof. Dr. Eberhard Neumann, Physical and Biophysical Chemistry, Faculty of Chemistry, University of Bielefeld, P. O. Box 100 131, D-33501 Bielefeld, Germany.

Phone: +49 521 106 20 53; Fax: +49 521 106 29 81

Abstract

The electroporative transfer of gene DNA and other bioactive substances into tissue cells by electric pulses gains increasing importance in the new disciplines of electrochemotherapy and electrogenetherapy. The efficiency of the electrotransfer depends crucially on the adsorption of the gene DNA and oligonucleotides to the plasma cell membranes. Here it is shown that the adsorption of larger oligonucleotides such as fragments (ca. 300 bp) of sonicated calf-thymus DNA, to anionic lipids of unilamellar vesicles (diameter Φ = 300 ± 90 nm) is greatly enhanced by divalent cations such as Ca^{2+}-ions. Applying centrifugation, bound and free DNA are monitored optically at the wavelength λ = 260 nm. Using arsenazo III as a Ca^{2+}-indicator and atomic absorption spectroscopy (AAS), Ca^{2+}-titrations of DNA and vesicles yield the individual equilibrium constants of Ca^{2+}- and DNA-binding not only for the binary complexes: Ca/lipids, Ca/DNA and DNA/lipids, respectively, but also for the various processes to form the ternary complex DNA/Ca/lipids. - The data provide the basis for goal-directed optimization protocols for the adsorption and thus efficient electrotransfer of oligonucleotides and polynucleotides into cells.

Introduction

The direct electrotransfer of “naked” gene DNA and other bioactive molecules into tissue cells is of crucial interest in the new medical disciplines of electrochemotherapy and electrogenetherapy [1]. The concept and technique of membrane electroporation (ME), introduced 1982 [2], gains increasing functional importance in medical therapies with minimum risk of undesired side effects [1, 3, 4]. The efficiency of the electrotransfer of oligonucleotides [5] and polynucleotides, especially at the lower, harmless field strengths of the applied electric pulses is greatly enhanced by prior adsorption of the bioactive polyelectrolytes on the cell membrane surfaces, before the actual therapeutic pulsing.

In order to quantify DNA adsorption to electrified cell surfaces, we use anionic lipid vesicle surfaces to mimic the lipid parts of cell plasma membranes for the Ca^{2+}-dependent binding of DNA. There are many studies on the interaction between Ca^{2+}-ions and lipid vesicles with different composition of lipids in the absence of DNA [6-9] or with DNA and zwitterionic and positively charged liposomes [10, 11]. Also the binding of different cations to DNA has been quantified previously [12-14]. Here, we address the thermodynamics of

ternary complexes in general and the ternary complex Ca/DNA/lipid vesicles, in particular. We continue to model the lipid part of curved cell membranes by spherical unilamellar lipid vesicles, using a mixture of 1 mM PS:2POPC (VET 400) which at pH 7.4 form negatively charged lipid surfaces providing electrified interfaces. Since DNA is a negatively charged polyelectrolyte, divalent cations such as Mg^{2+} and Ca^{2+} have been traditionally used to bridge the DNA with negatively charged cell membranes [2, 15, 16]. The formation of ternary complexes Ca/DNA/lipids is also indicated at the interface air/solution of lipid monolayers [17].

Here these interface complexes are further quantified. In detail, using centrifugation techniques, the individual equilibrium constants of Ca^{2+}- and DNA-binding are determined not only for the binary complexes: Ca/lipids, Ca/DNA and DNA/lipids, respectively, but also for the various processes to form the ternary complex DNA/Ca/lipids on the electrified lipid bilayer surface. The data provide chemical-compositional information for goal-directed optimization protocols for the adsorption of oligonucleotides and polynucleotides, to be used for the efficient electrotransfer into cells.

Materials and Methods

Synthetic palmitoyl-oleoyl-phosphatidylcholine (POPC) is from Lipoid GmbH (Ludwigshafen, Germany). Bovine brain extract type III (containing 80-85% phosphatidylserine (PS)), for the monolayer experiments, and synthetic PS (98% purity) are from Sigma Chemie GmbH (Deisenhofen, Germany). Unilamellar lipid vesicles of 1 mM PS:2POPC are prepared by the vesicle extrusion technique (VET) [18, 19]. Pressing the lipid mixture 21 times through a porous (400 nm) polycarbonate membrane in a LipoFast Extruder (Avestin/Milsch, Germany) yields vesicles with diameters of 300 ± 90 nm. In this way, the vesicle samples have been prepared for each individual total Ca^{2+} concentration [Ca_t] in the suspension. To avoid osmotic pressure problems, $CaCl_2$ is added to the buffer solution before the vesicle preparation to balance [Ca_t]. The DNA has been added to the vesicle suspension at various [Ca_t].

High polymeric deoxyribonucleates (DNA type I) from calf thymus (Sigma Chemie GmbH) has been used to obtain DNA fragments of lengths 102 ± 17 nm or 300 ± 50 bp (determined by gel electrophoresis) by 180 sonication cycles (à 30 s) within 90 minutes using an ultrasound transducer (Branson Sonic Power Company USA).

All solutions are 1 mM HEPES, pH 7.4 buffer, T = 293 K (20° C). The total lipid concentration is 1 mM, corresponding to a vesicle density of $6.6 \cdot 10^{11}$ per mL buffer solution. The number of DNA molecules, for instance at the lowest concentration 35.5 μM (bp) in molar base pairs (bp), refers to $7 \cdot 10^{13}$ DNA molecules per mL buffer.

The centrifugations have been performed at $2.3 \cdot 10^5$ g, 60000 rotations per min for 45 min. The total concentration of DNA in the supernatant, $[D_t]^{sup}$, is determined from the absorbance A_{260} at the wavelength $\lambda = 260$ nm using an UVIKON 943, double beam UV/VIS spectrophotometer (Kontron Instruments).

The Ca^{2+}-indicator arsenazo III (Ar) (Aldrich Chemical Company Inc.) is used to determine the concentration [Ca] of free Ca^{2+} in the supernatant. A 100 μM stock solution is diluted with Ca^{2+} solutions to a final concentration of [Ar] = 10 μM. The calibration curve is determined from the differences in the absorbances A_{602} at $\lambda = 602$ nm (Ca^{2+}-sensitive wavelength) of these samples and a sample with 1 mM EDTA ([Ca] = 0) [20].

Atomic absorption spectroscopy (AAS, PYE UNICAM SP 1900 (Philips GmbH, Kassel, Germany)) has been used to determine the total Ca^{2+} concentration in the supernatant. The calibration of the apparatus has been performed in two ranges. Standard calcium solutions have been obtained by dilution of a 1 M standard calcium stock solution. $LaCl_3$ (stock solution 10%) has been added to yield a final concentration of 1% La. The calcium content of the probe is determined by spraying aliquots of 190 μl into an air-acetylene flame and measuring the absorbance at the resonance line 422.7 nm. $LaCl_3$ has been also added to each supernatant sample (1%). A mean value from 3 measurements is used to quantify the total Ca^{2+} concentration, $[Ca_t]^{sup}$, in the supernatant.

The monolayer experiments have been carried out in a teflon trough (10 x 24 x 0.3; cm) from Riegler and Kirstein GmbH, Potsdam, Germany. The trough is filled with 1 mM HEPES, 10 mM NaCl, pH 7.4, T = 293 K (20° C). The Ca^{2+} concentration is varied with $CaCl_2$ in the range $0 \leq [Ca_t] / mM \leq 1$. The surface pressure is measured by the Wilhelmy method. After spreading 20 μL PS:2POPC (1 mg/mL) dissolved in n-hexane at the air-water interface and waiting for n-hexane evaporation, the surface pressure-area isothermes are recorded. In the case of 1 mM $CaCl_2$ and 35.5 μM (bp) DNA, the DNA is added together with the buffer in the subphase. The π/A isothermes are recorded 10 times and a mean isotherm is documented.

Results

Monolayer/DNA interaction

In Fig. 1, typical surface pressure/area isothermes of a lipid mixture PS:2POPC are shown. In the case of $[Ca_t] = 0$, the collapse point is given by A_{coll} ($[Ca_t] = 0$) = 92 cm^2. At $[Ca_t] = 0.5$ mM, A_{coll} ($[Ca_t] = 0.5$ mM) = 93 cm^2; the isotherms are almost identical. However, at $[Ca_t] = 1$ mM, the collapse point is shifted to the lower value A_{coll} ($[Ca_t] = 1$ mM) = 82 cm^2. When 35.5 μM (bp) DNA is added into the subphase at $[Ca_t] = 1$ mM the collapse area A_{coll} ($[Ca_t] = 1$ mM; DNA) = 97.5 cm^2 is larger than that for $[Ca_t] = 0$.

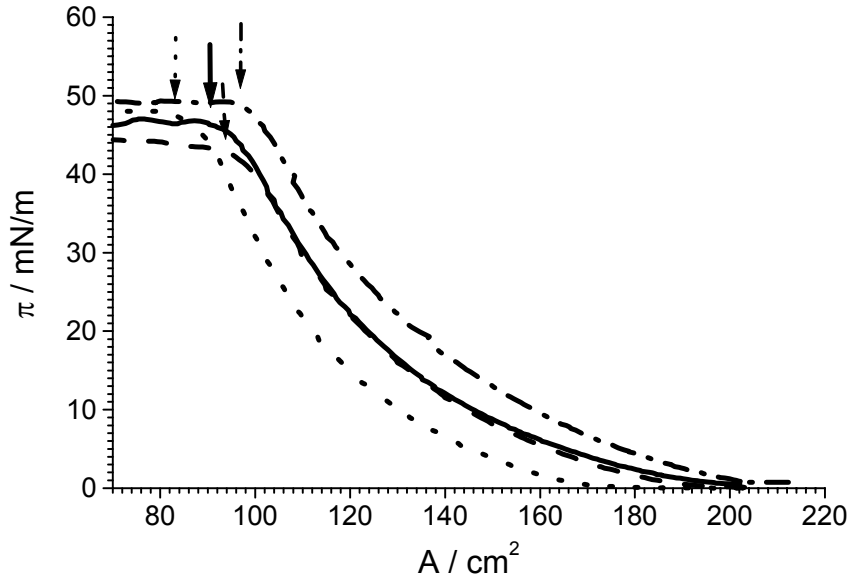

Fig. 1 Surface pressure (π)-area (A) isotherms of the lipid mixture PS:2POPC (1 mg/ml) in n-hexane spread at the air-water interface and subphases at the conditions $[Ca_t]$ /mM = 0 (—), 0.5 (– –), 1 (- - -), without DNA and $[Ca_t] = 1$ mM (— -) with 35.5 μM (bp) DNA, T = 293 K (20^0 C), 1 mM Hepes, 10 mM NaCl, pH 7.4. The arrows indicate the collapse points.

Optical densities of the suspensions

As seen in Fig. 2, the optical density, OD_{365}, at the wavelength λ = 365 nm of a vesicle suspension increases with increasing $[Ca_t]$. It is noted that the data points of the two documented sets refer to samples which are separately extruded at the given $[Ca_t]$-values, respectively. The data scatter within the indicated range. OD_{365} will be used to determine the equilibrium constant for the binding of Ca^{2+} to the vesicle surface.

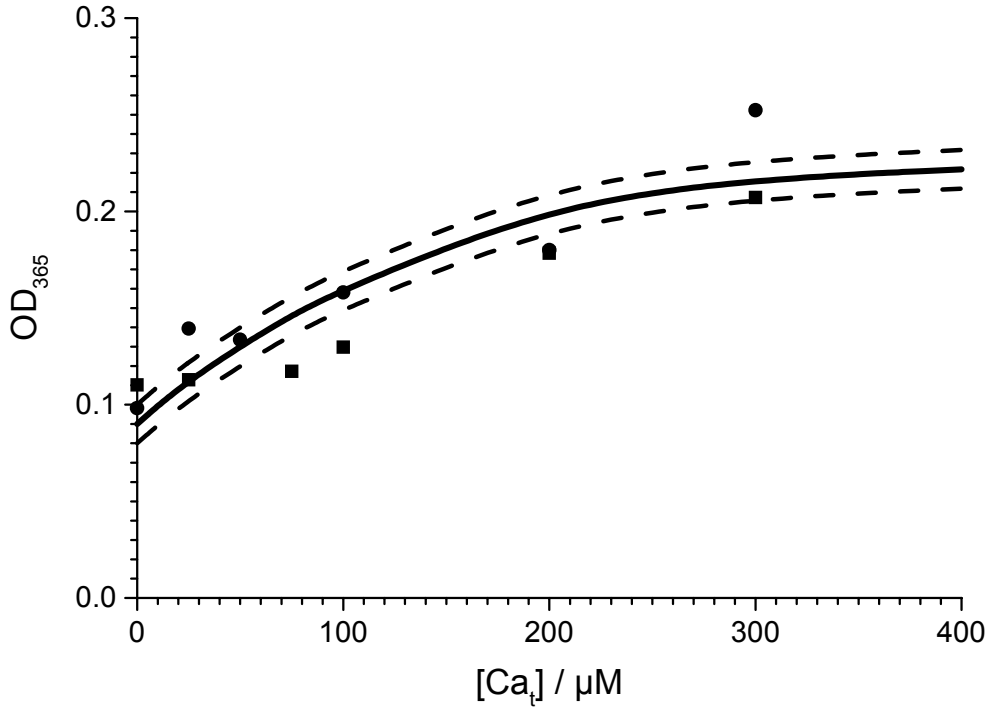

Fig. 2 Spectrophotometric (OD_{365}) Ca^{2+}-titration of two selected sets of vesicle preparations. The data of set 1 (■) and set 2 (●) refer each to a given $[Ca_t]$, respectively. The difference $\Delta OD = OD_{365} - OD^0_{365}$ is assumed to be proportional to Ca^{2+} bound $[Ca_b]$. The initial $OD^0_{365} = 0.09 \pm 0.02$ refers to Ca^{2+} bound at $[Ca_t] = 0$. The apparent maximum $OD^{max}_{365} = 0.23 \pm 0.02$ refers to $[Ca_b]^{max}$. The dashed lines represent the data fit with Eq. (10) of the text, yielding the equilibrium constant $K^0_{Ca} = 15 \pm 5$ µM at 1 mM HEPES, pH 7.4, T = 293 K (20^0 C). The full thick line represents the mean of the fitting line for the two documented, separated data sets.

Ca^{2+}-binding to DNA

The absorbance A_{260} of DNA at the wavelength $\lambda = 260$ nm (absorbance maximum) is traditionally used to calculate the concentration of DNA and to indicate interactions of DNA with other substances. Generally, the concentration [D] of DNA in solution is calculated from Lambert-Beer's law according to:

$$[D] = A_{260} / \varepsilon \cdot d \qquad (1)$$

where d is the optical path length and ε is the absorption coefficient at $\lambda = 260$ nm. In buffer solution, the absorption coefficient of the free DNA double strand is given by $\varepsilon_D = 13200$ $M^{-1}cm^{-1}$, where [D] refers to molarity in base pairs (bp). In Fig. 3, A_{260} decreases with increasing total Ca^{2+} concentration $[Ca_t]$, starting at $[Ca_t] = 0$, where we assume that the

degree of binding $\beta_{CaD} = 0$, down to apparent saturation A_{min} referring to $\beta_{CaD} = 1$, yielding $\varepsilon_{CaD} = 12600\ M^{-1}cm^{-1}$.

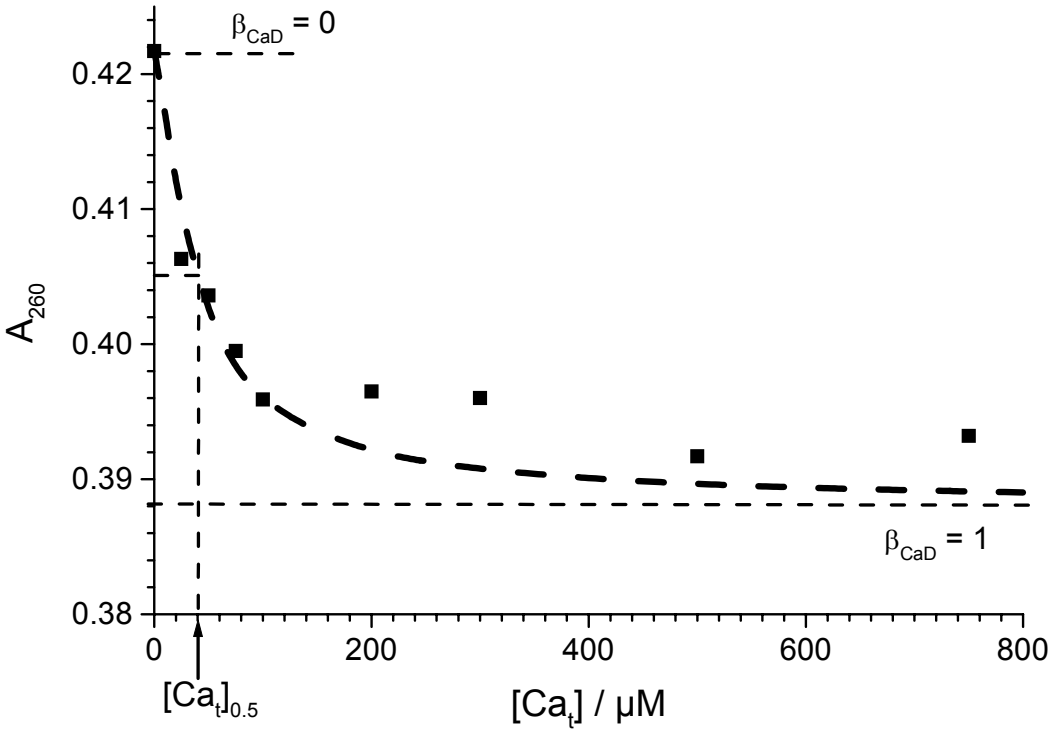

Fig. 3 Spectrophotometric (A_{260}) Ca^{2+}-titration of a DNA solution at $[D_t] = 32$ µM (bp). Here the initial absorbance $A_0 = 0.422 \pm 0.002$ refers to the degree of Ca^{2+}-binding to DNA $\beta_{CaD} = 0$. The estimated saturation value $A_{min} = 0.388 \pm 0.002$ refers to $\beta_{CaD} = 1$. The full dashed line represents the data fit with Eq. (13) of the text, yielding the equilibrium constant $K^0_{CaD} = 24 \pm 5$ µM at 1 mM HEPES, pH 7.4, T = 293 K (20^0 C).

Ternary complex DNA/Ca/lipids

The Ca^{2+}-titrations of lipid vesicles in the presence of DNA of total concentration $[D_t]$ in the suspension show that the absorbance $A_{260}([D_t]) = OD_{260}(Ves+[D_t]) - OD_{260}(Ves)$ changes differently with increasing total Ca^{2+} concentration $[Ca_t]$, see Fig. 4 **A**. The A_{260}-values are calculated from the differences of the optical densities $OD_{260}(Ves+[D_t])$ in the presence of DNA and vesicles, and that in the absence of DNA, respectively. As already seen in Fig. 3, $A_{260}([D_t])$ of DNA in the absence of vesicles reflects both the complexed DNA and free DNA starting with $A_0 = \varepsilon_D \cdot d \cdot [D_t]$ and heading at the saturation value $A_{min} = \varepsilon_{CaD} \cdot d \cdot [D_t]$, where all DNA is complexed; see below.

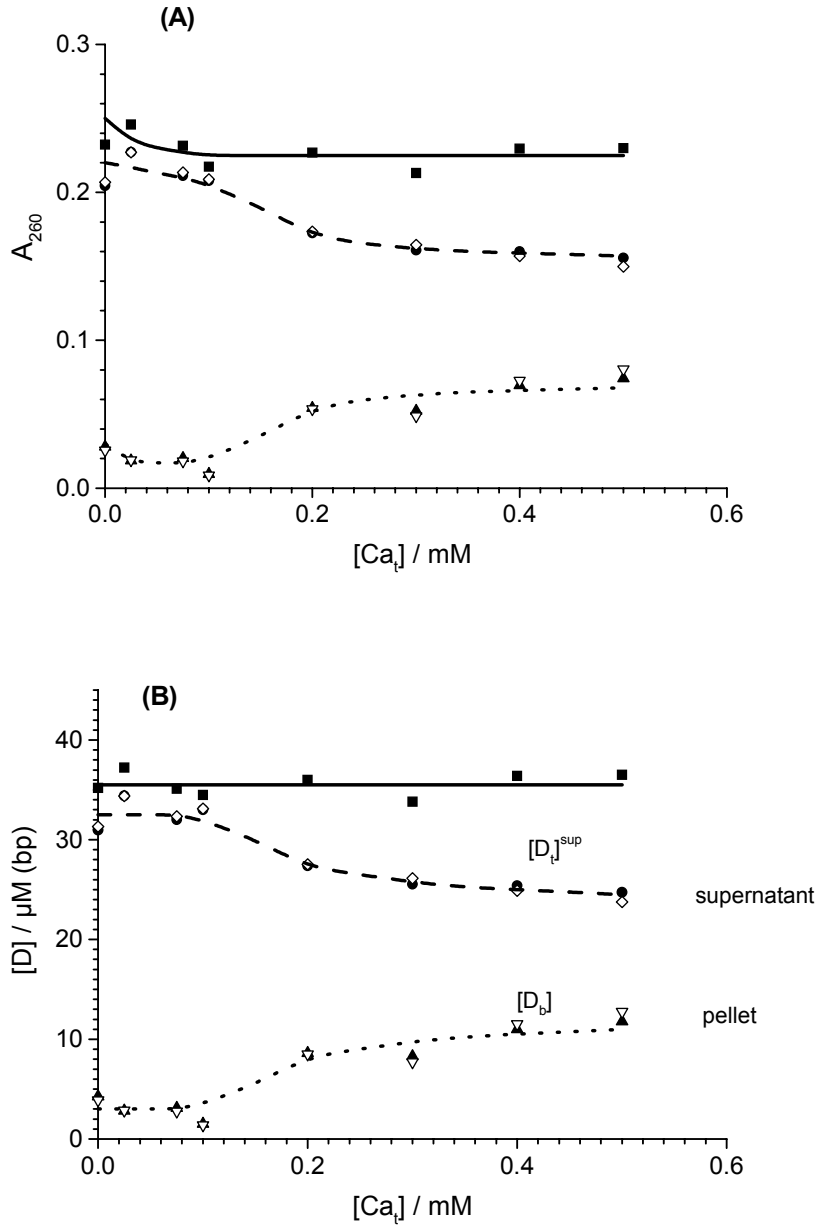

Fig. 4 Ca^{2+}-titration of the DNA/vesicle suspension at $[D_t]$ = 35.5 µM (bp) and of the supernatant (sup), respectively. Measured data points **(A)**: (■) $A_{260}([D_t]) = OD_{260}(Ves+[D_t]) - OD_{260}(Ves)$ of the suspension; (●), (◇) $A_{260}([D_t]^{sup})$ refer to the supernatant. The values (▲), (▽) are calculated from $A_{260}([D_b]) = A_{260}([D_t]) - A_{260}([D_t]^{sup})$ of the pellet. **(B)**: (■) $[D_t]$, calculated with Eq. (1) of the text; (●), (◇) refer to the total DNA ($[D_t]^{sup} = [D] + [CaD]$) in the supernatant; (▲), (▽) refer to the calculated concentration ($[D_b] = [DB] + [DCaB]$) of bound DNA in the pellet. Note, that the data points at the various $[Ca_t]$ refer to aliquots of the same vesicle preparation, the supernatant data to two aliquots at a given $[Ca_t]$. T = 293 K (20^0 C), 1 mM HEPES, pH 7.4.

The absorbance $A_{260}([D_t]^{sup})$ of the supernatant of the centrifuged mixture of vesicles decreases after a 'delay' range of $0 \leq [Ca_t]/mM < 0.1$, tending finally to an apparent saturation value. The difference $A_{260}([D_b]) = A_{260}([D_t]) - A_{260}([D_t]^{sup})$ reflects the increase of bound DNA with increasing $[Ca_t]$. If higher concentrations of DNA are used, all A_{260}-values are larger, but the relative changes with increasing $[Ca_t]$ are the same as for the lowest DNA concentration with $[D_t] = 35.5$ μM (bp). Using Eq. (1), the quantities A_{260} of Fig. 4 **A** are converted to the respective concentrations: $[D_t]$ and $[D_t]^{sup}$ of Fig. 4 **B**. Mass conservation dictates that the bound DNA is given by:

$$[D_b] = [D_t] - [D_t]^{sup}. \quad (2)$$

In Fig. 4 **B**, it is seen that $[D_b]$ sigmoidally (delay) increases and then appears to saturate with increasing $[Ca_t]$. Note that already at $[Ca_t] = 0$, there is some DNA bound to the vesicle surface, denoted by $[D_b^0]$.

Determination of [Ca] with arsenazo III (Ar)

The Ca^{2+}-indicator arsenazo III is traditionally used for the optical indication of Ca^{2+} at the wavelength $\lambda = 602$ nm [21]. Here, we apply Ar to the supernatant of the centrifuged samples. First the absorbance A_{602} of a solution of $[Ar] = 10$ μM is measured as a function of $[Ca_t]$ to yield an optical calibration curve (data not shown). Formally, the assumption of a simple stoichiometry Ca:Ar = 1:1 [20, 22] is sufficient to estimate the concentration [Ca] of free Ca^{2+} according to the mass conservation:

$$[Ca] = [Ca_t] - [CaAr] = [Ca_t] - \beta_{CaAr}[Ar_t] \quad (3)$$

where the degree of Ca^{2+} bound to Ar is given by:

$$\beta_{CaAr} = \frac{[CaAr]}{[Ar_t]} = \frac{[Ca]}{[Ca] + K_{CaAr}} = \frac{\Delta A_{602}}{\Delta A_{602}^{max}} \quad (4)$$

It is readily shown that the concentration of free Ca^{2+} is given by:

$$[Ca] = \frac{1}{2}[([Ca_t] - [Ar_t] - K_{CaAr}) + X] \quad (5)$$

where $X = \sqrt{([Ca_t] + [Ar_t] + K_{CaAr})^2 - 4 \cdot [Ca_t] \cdot [Ar_t]}$.

As expected, $[Ca] = [Ca_t]$ for a solution without DNA and without vesicles. See the Fig. 1A of the appendix.

The total Ca^{2+} concentration in the supernatant by AAS

The calibration line, $A_{422.7}$ versus $[Ca_t]^{sup}$, at the resonance line for Ca^{2+}, $\lambda = 422.7$ nm, is established with standard solutions containing 1% (weight) La^{3+} for the two concentration

ranges: $0 \leq [Ca_t] / \mu M \leq 100$ and $100 \leq [Ca_t] / \mu M \leq 500$ (data not shown). The La^{3+}-ions displace Ca^{2+}-ions from the binding sites and make them available for the AAS measurements in the supernatant [23, 24].

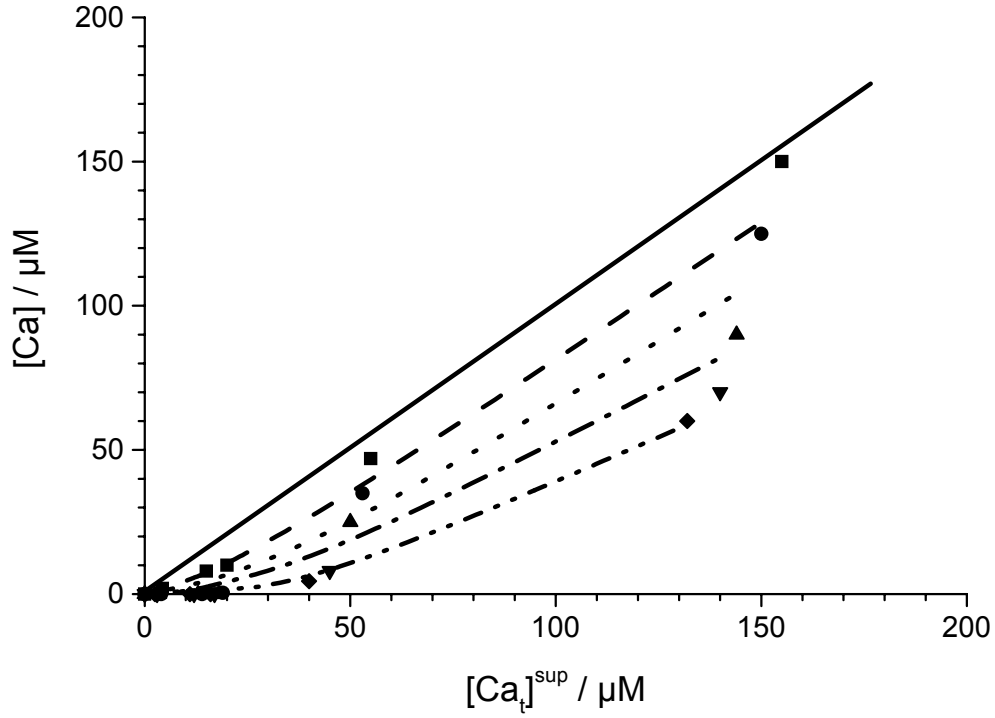

Fig. 5 Ca^{2+}-binding isotherms. [Ca] versus $[Ca_t]^{sup} = [Ca] + [CaD]$ in the supernatant of the centrifuged vesicle suspensions for different DNA concentrations: $[D_t] / \mu M$ (bp) = (■) 0, (●) 35.5, (▲) 71, (▼) 107 and (◆) 143; from top to bottom. The data fit, using Eq. (12) of the text with $[CaD]^{max} = [D_t]^{sup}$, yields $K^0_{CaD} = 24 \pm 5$ μM at T = 293 K (20^0 C), 1 mM HEPES, pH 7.4. The straight full line refers to: $[Ca] = [Ca_t]^{sup}$ at $[D_t] = 0$.

As seen in Fig. 5, at a given $[Ca_t]^{sup}$, [Ca] in the supernatant decreases with increasing amounts of DNA $[D_t]$ in the suspension. Comparisons refer to the same $[Ca_t]^{sup}$ consistent with $[Ca] = [Ca_t]^{sup} - [CaD]$. As expected, with increasing concentration of free DNA, [D], in the supernatant, the concentration [CaD] is also increasing. In the case of vesicle suspensions without DNA, the equality $[Ca_t]^{sup} = [Ca]$ holds (straight full line). The scatter of the data points is relatively large, because two methods are used to determine the Ca^{2+} concentrations in the supernatant. $[Ca_t]^{sup}$ is measured by AAS and [Ca] is determined by using arsenazo III as an optical indicator.

Data Evaluation and Discussion

Evidence for DNA binding to a PS:2POPC lipid monolayer

As recalled from Fig. 1, the monolayer data exhibit different values for the collapse area in the π/A isotherms. The area per molecule at collapse, a_{coll}, is calculated according to:

$$a_{coll} = A_{coll} / N = A_{coll} \cdot \overline{M} / (N_A \cdot c \cdot V) \qquad (6)$$

from the experimental collapse area, A_{coll}, of the lipid film. N_A is the Avogadro constant, $\overline{M}$ = 784,06 g/mol is the average molar mass of a lipid in the mixture PS:2POPC, N the number of lipid molecules in the mixture, c = 1 mg/ml the mass concentration and V = 20 µl the volume of the lipid solution spread on the surface. The areas per molecule occupied by the lipids are: $a_{coll}([Ca_t] = 0) = 0.6$ nm^2, $a_{coll}([Ca_t] = 0.5$ mM$) = 0.605$ nm^2 and $a_{coll}([Ca_t] = 1$ mM$) = 0.535$ nm^2. The quantities $a_{coll} = 0.58$ nm^2 for PC and $a_{coll} = 0.574$ nm^2 for PS have been obtained by NMR studies [25]. A value of 0.42 nm^2 has been found for DMPC [26].

The decrease of the area per molecule at collapse in the presence of Ca^{2+}-ions (see also Huster et al. [25]) is consistent with the binding of the divalent cations to the negatively charged groups of phosphatidylserine [27], leading to a denser packing of the lipids in the monolayer films; hence a smaller area is occupied by one lipid molecule. When DNA is added to the aqueous phase at $[Ca_t] = 1$ mM, the area per molecule increases up to 0.635 nm^2, indicating DNA inserting into the lipid film. It appears that DNA binds at the lipid monolayer interface through Ca^{2+}-ions, providing indirect evidence for the ternary complex Ca/DNA/lipids.

Overall scheme for the Ca^{2+} and DNA binding reactions

Fig. 6 displays the overall scheme for the various binary complexes and the ternary complex DNA/Ca/B, where B refers to binding sites on the vesicle surface. In detail, DNA (D), Ca^{2+}-ions and the binding sites B on the surface of the vesicles form the complex DCaB along different pathways. The scheme expresses all binding steps as 1:1 complexes. Note that D refers to one base pair (bp) and B to probably two charged lipid head groups (of two PS molecules).

The apparent dissociation equilibrium constants of the binary complexes are defined as:

$$K^0_{Ca} = [Ca] \cdot \frac{[B]}{[CaB]}, \quad K^0_{CaD} = [Ca] \cdot \frac{[D]}{[CaD]}, \quad K^0_{D} = [D] \cdot \frac{[B]}{[DB]} \qquad (7)$$

respectively. The three different ternary complex formations are characterized by:

$$K'_D = [D]\cdot\frac{[CaB]}{[DCaB]}, \quad K'_{CaD} = [CaD]\cdot\frac{[B]}{[DCaB]}, \quad K'_{Ca} = [Ca]\cdot\frac{[DB]}{[DCaB]}. \tag{8}$$

The individual reaction steps are treated now separately.

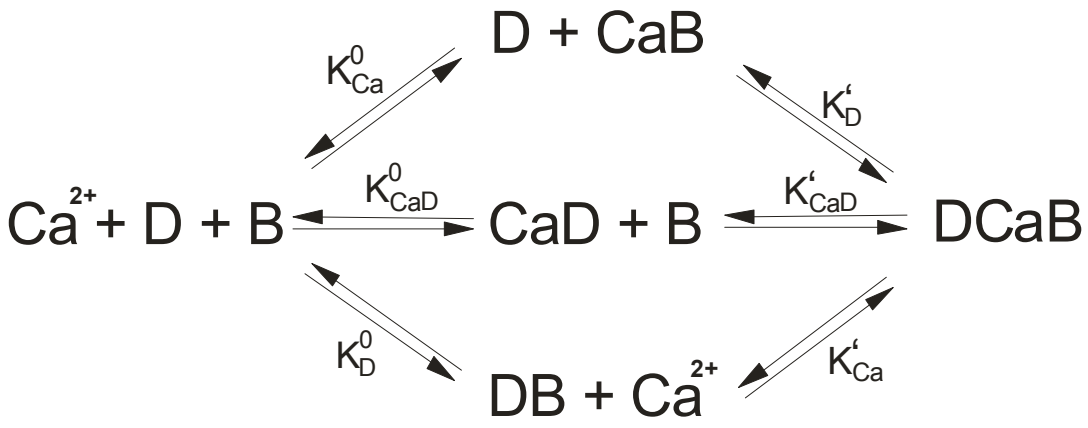

Fig. 6 Overall cyclic reaction scheme for the binding of Ca^{2+}-ions to DNA (D) and to B-sites on the lipid vesicle surface, leading to the various binary complexes and the ternary complex DCaB on the outer vesicle surface. The B-sites for the binding of DNA and Ca^{2+} are the anionic head groups of the lipids.

Ca^{2+}-binding to sites B on the vesicle surface

In the absence of DNA, the binding of Ca^{2+} to surface sites B is described by: $Ca + B \rightleftharpoons CaB$, where B represents one or more anionic lipid head groups. Written in dissociation direction, we have:

$$CaB \rightleftharpoons Ca + B \tag{9}$$

characterized by the dissociation equilibrium constant K^0_{Ca}, defined by Eq. (7). The degree of Ca^{2+}-binding, β_{Ca}, to B-sites on the vesicle surface is given by:

$$\beta_{Ca} = \frac{[Ca_b]}{[Ca_b]^{max}} = \frac{[CaB]}{[B_t]} = \frac{[Ca]}{[Ca] + K^0_{Ca}} \tag{10}$$

where $[B_t]$ is the total concentration of B-sites. The differences in the optical densities (turbidities), $\Delta OD_{365} = OD_{365} - OD^0_{365}$ and $\Delta OD^{max}_{365} = OD^{max}_{365} - OD^0_{365}$ (Fig. 2), where OD^0_{365} refers to $[Ca_t] = 0$, are used to determine $\beta_{Ca} = \Delta OD_{365} / \Delta OD^{max}_{365}$. In Eq. (10), $[Ca_b]$ is

the concentration of bound Ca^{2+} in the pellet, $[Ca_b]^{max}$ is the maximal concentration term and [Ca] is determined in the supernatant (by AAS and with arsenazo III).

As seen in Fig. 2, the data fit using Eq. (10) faces the problem of large data scatter, inherent in the method of vesicle preparation and handling as a pellet and the supernatant. Nevertheless, the fit yields reliably $K^0_{Ca} = 15 \pm 5$ μM and $[Ca_b]^{max} = 170 \pm 20$ μM at T = 293 K (20^0 C), 1 mM HEPES, pH 7.4.

Tab. 1 Apparent dissociation equilibrium constants of the binding of Ca^{2+} to lipids

K^0_{Ca}	Lipid composition	Buffer	Reference
0.07 μM (7 mN/m) 0.035 μM (32.4 mN/m)	PS (monolayer)	Distilled water, T = 293 K (20^0 C)	[29]
6 μM	PS (bilayer, vesicles)	1 mM Ca^{2+}, T = 293 K (20^0 C)	[9]
98 μM 100 μM 79 μM 85 μM	PA/PS (1:5) PA/PS (1:2) PA/PS (4:5) PC/PS	145 mM NaCl, pH 7.4, T = 293 K (20^0 C)	[30]
83.3 mM 27.7 mM	PS (vesicle)	100 mM NaCl, pH 7.5, T = 293 K (20^0 C) 10 mM NaCl, pH 7.5, T = 293 K (20^0 C)	[8]
28.6 mM	PS (vesicle)	100 mM NaCl, 2 mM L-histidine, 2 mM TES, pH 7.4, T = 293 K (20^0 C)	[6]
265 μM	PS (vesicle)	100 mM NaCl, pH 7.4, T = 293 K (20^0 C)	[7]
124 mM	PC/PE/PS (4:4:1) multilamellar liposomes	100 mM NaCl, 10 mM Hepes, pH 7.4, T = 298 K (25^0 C)	[25]
1.8 ± 0.3 mM	Yeast cells	1 mM sorbitol, 1 mM Tris-HCl, pH 7.4 T = 293 K (20^0 C)	[16]
39.5 mM	Neuroblastoma cells	Dulbecco's, Eagle's	[31]

For consistency check, two other methods, AAS and arsenazo III, have been used to determine the dissociation equilibrium constant K^0_{Ca} and $[Ca_b]^{max}$ in the pellet; here $[Ca_t]^{sup}$ =

[Ca]. See the Fig. 2A of the appendix. The data fit for the relation $[Ca_b] = [Ca_t] - [Ca]$ versus [Ca] yields the same values for K_{Ca}^0 and $[Ca_b]^{max}$ as obtained from the spectrophotometric Ca^{2+}-titration of the vesicles.

If B for the binding of Ca^{2+} refers to 2 anionic PS molecules, the maximum concentration of the bound Ca^{2+} on the vesicle surface is $[Ca_b]^{max} = [Ca(PS)_2]^{max} = [PS_b]^{max}/2$; that is approximately equal to half the concentration of complexed (or bound) PS on the vesicle membrane. With the total lipid concentration $[L_t]$ = 1 mM, we obtain $[PS] = [L_t]/3$ = 0.33 mM. Since DNA-binding in the titration method occurs only on the outside monolayer of the vesicle bilayer, the head group concentration available for the DNA/Ca/PS complexation on the outside is [PS]/2 = 0.165 mM.

A survey of the binding of Ca^{2+}-ions to membrane surfaces, modelled by monolayers, bilayers and lipid vesicles, indicates largely different equilibrium constants. Note that apparent equilibrium constants are dependent on the ionic strength. In particular, when [NaCl] decreases from 100 mM to 10 mM, the apparent dissociation constant of the Ca/PS system decreases about two orders of magnitude [8], [28]. See Tab. 1.

The binding of Ca^{2+} to DNA

The binding of Ca^{2+} to DNA in solution (without vesicles)

If the binding of Ca^{2+} to DNA (D) is specified as a dissociation reaction according to:

$$CaD \rightleftharpoons Ca + D, \tag{11}$$

the degree of Ca^{2+} binding to DNA in solution is defined as:

$$\beta_{CaD} = \frac{[CaD]}{[CaD]^{max}} = \frac{[Ca]}{[Ca] + K_{CaD}^0} \tag{12}$$

where K_{CaD}^0 is the respective apparent equilibrium constant (Eq. (7)) and β_{CaD} is obtained from the absorbance ratio according to $\beta_{CaD} = \Delta A / \Delta A_0 = (A_0 - A)/(A_0 - A_{min})$ (Fig. 3). Note that D represents two neighbouring phosphate residues or, formally, one base pair. Here, the maximum concentration $[CaD]^{max}$, of the CaD complex is approximated by $[CaD]^{max} = [D_t]$. The data (Fig. 3) are evaluated according to:

$$A - A_{min} = (A_0 - A_{min}) \frac{K_{CaD}^0}{[Ca] + K_{CaD}^0}. \tag{13}$$

with A_0 = 0.422 ± 0.002 and A_{min} = 0.388 ± 0.002. K_{CaD}^0 is calculated from the half-point at $\beta_{CaD} = 0.5$, using:

$$K_{CaD}^0 = [Ca]_{0.5} = [Ca_t]_{0.5} - [D_t]/2. \tag{14}$$

In the example shown in Fig. 3, $[Ca_t]_{0.5} = 40 \pm 5$ μM and thus $K^0_{CaD} = 24 \pm 5$ μM at T = 293 K (20° C), 1 mM HEPES, pH 7.4.

The binding of Ca^{2+} to DNA in the supernatant

In the presence of vesicles, the Ca^{2+}-binding to DNA is evaluated from the supernatant data. The equilibrium constant K^0_{CaD} is related to β_{CaD} with the specification $[CaD]^{max} = [D_t]^{sup}$; Eq. (12).

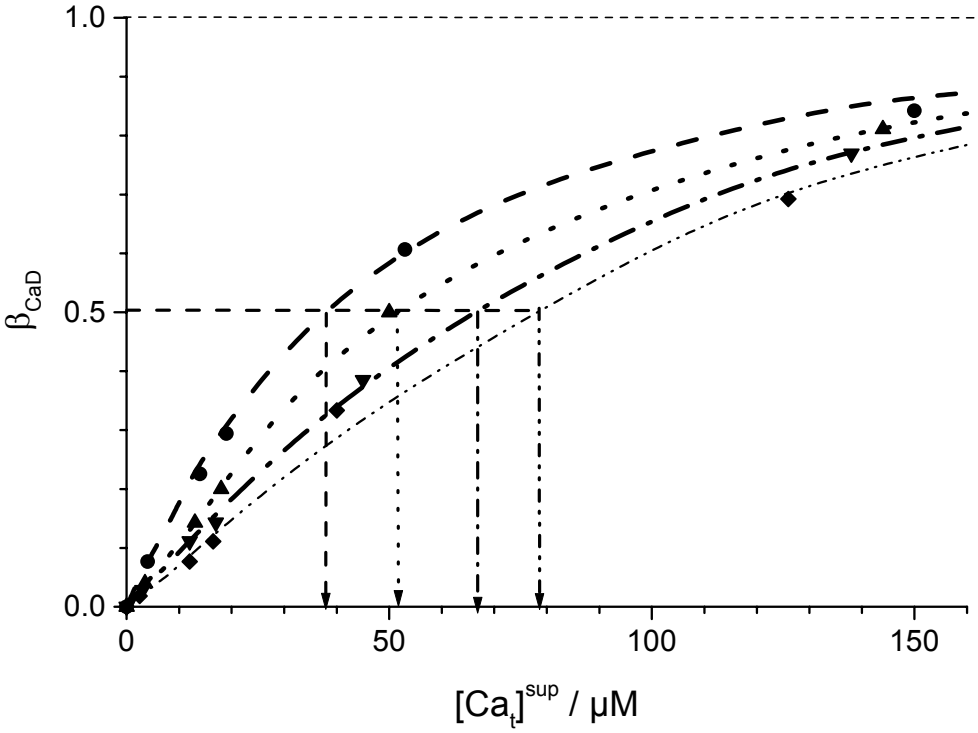

Fig. 7 The degree of binding β_{CaD} in the supernatant, calculated with Eq. (12) (or (A2) of the appendix) at $[D_t]$ / μM (bp) = (●) 35.5, (▲) 71, (▼) 107 and (◆) 143. $[D_t]$ refers to the total concentration of DNA in the vesicle suspensions. The arrows represent $[Ca_t]^{sup}$ at $\beta_{CaD} = 0.5$.

Graphically (Fig. 7), for a given total DNA concentration, $[D_t]^{sup}$, in the supernatant, the equilibrium constant K^0_{CaD} is determined from the half-points at $\beta_{CaD} = 0.5$. See Eq. (A2) of the appendix. There is another consistency check for the determination of K^0_{CaD} according to the relationship:

$$K^0_{CaD} = [Ca]\left(\frac{[D_t]^{sup}}{[Ca_t]^{sup} - [Ca]} - 1\right) \tag{15}$$

which is obtained from Eq. (12) by using $[CaD]^{max} = [D_t]^{sup}$ and mass conservation according to: $[CaD] = [Ca_t]^{sup} - [Ca]$. See the Fig. 3A of the appendix. The calculation yields $K^0_{CaD} = 26 \pm 6$ µM, being close to $K^0_{CaD} = 24 \pm 5$ µM from Fig. 3. Previous documentations of Ca/DNA dissociation equilibrium constants strongly vary. Apparent dissociation constants of 0.3 mM and 0.5 mM have been reported for DNA from *Micrococcus lysodeikticus* in 50 mM electrolyte solution at 23° C [12]. The equilibrium constant of 7.14 µM in 5 mM Tris and 50 mM NaCl obtained for the binding of Ni(II)-ions to calf thymus DNA [13] is comparable with $K^0_{CaD} = 24 \pm 5$ µM found here. Generally, however the binding of divalent ions to DNA is sensitive to both the type of divalent ions [13] and the ionic strength.

Overall DNA-binding to sites B on the vesicle and to the complex CaB

It is appropriate to describe the overall binding of DNA by the overall reaction scheme:

$$D + (B + CaB) \rightleftharpoons (DB + DCaB) \tag{16}$$

where the Ca^{2+}-dependent overall dissociation equilibrium constant is given by:

$$\overline{K'^{(Ca)}_D} = [D] \cdot \frac{[B] + [CaB]}{[DB] + [DCaB]} = [D] \cdot \frac{1 - \overline{\beta_D}}{\overline{\beta_D}} = [D]_{\overline{\beta_D} = 0.5} \tag{17}$$

and the overall degree of binding $\overline{\beta_D}$ refers to:

$$\overline{\beta_D} = \frac{[DB] + [DCaB]}{([DB] + [DCaB])^{max}} = \frac{[D_b]}{[D_b]^{max}} = \frac{[D]}{[D] + \overline{K'^{(Ca)}_D}} \ , \tag{18}$$

where $[D_b]^{max} = [B^D_t]$ is the total concentration of B sites available for the DNA-binding on the vesicle surface. The concentration [D] of free DNA in the supernatant decreases with increasing concentration [Ca] of free Ca^{2+} in the supernatant, as expected in line with the relationship:

$$[D] = [D_t]^{sup} \cdot \frac{K^0_{CaD}}{[Ca] + K^0_{CaD}} \tag{19}$$

obtained by substitution of $[CaD]^{max} = [D_t]^{sup}$ and $[CaD] = [D_t]^{sup} - [D]$ in Eq. (12). See the Fig. 4A of the appendix. The overall equilibrium constant $\overline{K'^{(Ca)}_D}$ can also be expressed as:

$$\overline{K'^{(Ca)}_D} = K'_D \cdot \frac{[Ca] + K^0_{Ca}}{[Ca] + K'_{Ca}} . \tag{20}$$

Eq. (20) is derived from Eq. (17); see Eq. (A4) of the appendix. In the case $[Ca_t] = 0$ (full line in Fig. 8), the reaction scheme (16) reduces to:

$$D + B \rightleftharpoons DB \tag{21}$$

and Eq. (20) yields:

$$\overline{K'_D}^{(Ca)} = K'_D \cdot K^0_{Ca} / K'_{Ca} = K^0_D, \tag{22}$$

where $K^0_D (= [D]\cdot[B]/[DB])$ refers to the adsorption of DNA to lipid surfaces in the absence of added Ca^{2+}-ions [32].

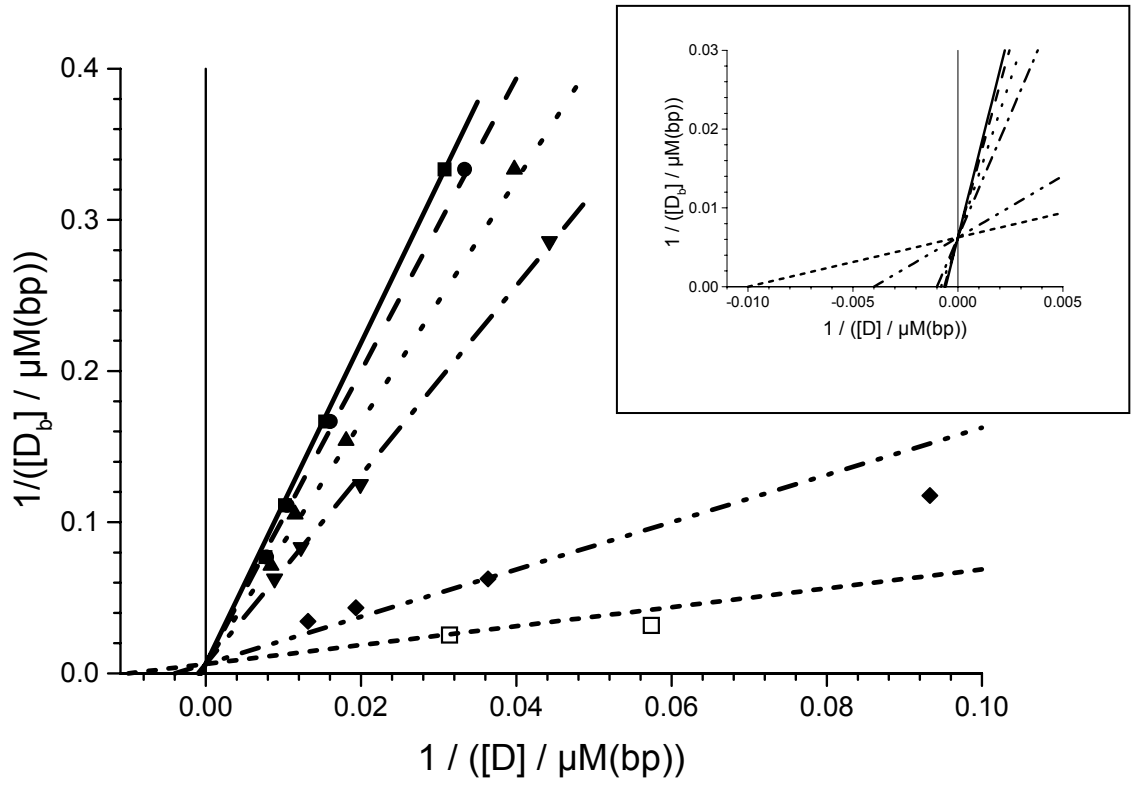

Fig. 8 The graphical determination of $[D_b]^{max}$ and $\overline{K'_D}^{(Ca)}$ from the double-reciprocal relationship according to Eq. (23) for $[Ca_t]$ / µM = (■) 0, (●) 25, (▲) 75, (▼) 100, (◆) 200 and (□) 300. The insert shows the enlarged intercept and the abscissa intersections.

Rearranging now Eq. (18) as a double-reciprocal relationship we obtain:

$$\frac{1}{[D_b]} = \frac{1}{[B^D_t]} \cdot \left(1 + \frac{\overline{K'_D}^{(Ca)}}{[D]}\right), \tag{23}$$

for different $[Ca_t]$ of the suspension (Fig. 8). In the case of DNA binding in the absence of Ca^{2+}-ions ($[Ca_t] = 0$), we obtain the solid line in Fig. 8. The intercept yields the common value $[B^D_t] = 160 \pm 20$ µM and the abscissa yields the various numerical values of $\overline{K'_D}^{(Ca)}$. The

concentration $[B_t^D]$ of binding sites for DNA is approximately equal to the maximum concentration, $[Ca_b]^{max}/2$, represented by the head group concentration [PS]/2 of PS available at the outer vesicle surface. For $\overline{K'^{(Ca)}_D} = [D]_{\overline{\beta_D} = 0.5}$, at each value of $[Ca_t]$ and at the half–point of bound DNA, $[D_b]_{0.5} = [D_b]^{max}/2 = [B_t^D]/2 = 80\ \mu M$, we obtain the respective value for the DNA-binding (data not shown) and a value $[Ca]_{0.5}$ of the free Ca concentration at $\overline{\beta_D} = 0.5$ according to:

$$[Ca]_{0.5} = K^0_{CaD} \cdot ([D_t]^{sup}_{0.5}/[D]_{0.5} - 1)\,. \qquad (24)$$

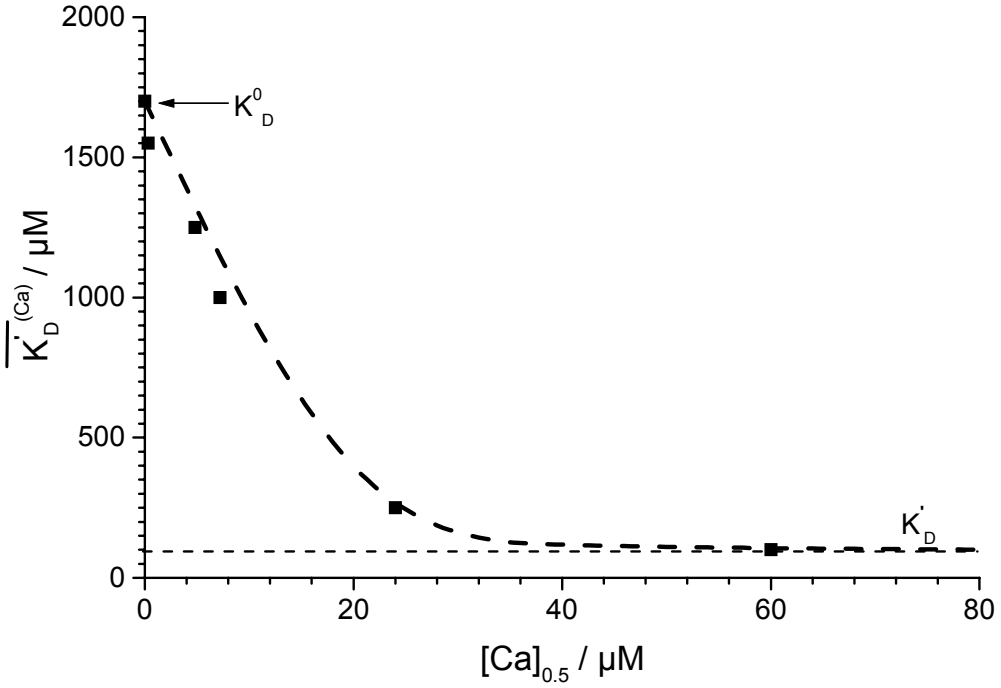

Fig. 9 The overall equilibrium constants $\overline{K'^{(Ca)}_D} = K'_D([Ca] + K^0_{Ca})/([Ca] + K'_{Ca})$ obtained from the abscissa intercepts in Fig. 8. The data fit with Eq. (20) yields $K^0_D = 1.7 \pm 0.1$ mM (bp) and $K'_D = 85 \pm 15$ µM (bp) at T = 293 K (20^0 C), 1 mM HEPES, pH 7.4.

Again, Eq. (24) is obtained by substitution of $[CaD]^{max} = [D_t]^{sup}$ and $[CaD] = [D_t]^{sup} - [D]$ into Eq. (12). In Fig. 9, it is seen that $\overline{K'^{(Ca)}_D}$ decreases with increasing half-point concentration $[Ca]_{0.5}$, according to Eq. (20) with $K^0_{Ca} \gg K'_{Ca}$. At [Ca] = 0, $\overline{K'^{(Ca)}_D} = K'_D \cdot K^0_{Ca}/K'_{Ca} = K^0_D$ and at $[Ca] \gg K^0_{Ca}$ and $[Ca] \gg K'_{Ca}$, we have $\overline{K'^{(Ca)}_D} = K'_D$. The data fit with Eq. (20) yields $K^0_D = 1.7 \pm 0.1$ mM (bp) and $K'_D = 85 \pm 15\ \mu M$ (bp) at T = 293 K (20^0C), 1 mM HEPES, pH

7.4. The results are in line with $K^0_{Ca} = 24 \pm 5\ \mu M$, being indeed larger than $K'_{Ca} = 0.75 \pm 0.25\ \mu M$; see below. As a further consistency check, the values of $\overline{K'^{(Ca)}_D}$ are calculated for each value of $[D_b]$, $[D_t]^{sup}$ and [Ca]. Introducing Eq. (19) into Eq. (23), rearrangement yields:

$$\overline{K'^{(Ca)}_D} = \left(\frac{[B^D_t]}{[D_b]} - 1\right) \cdot \frac{[D_t]^{sup} \cdot K^0_{CaD}}{[Ca] + K^0_{CaD}}. \tag{25}$$

Data fit analogous to the data fit with Eq. (20) yields K'_D = 85 ± 15 μM (bp) and K^0_D = 1.7 ± 0.1 mM (bp). See the Fig. 5A of the appendix. The results are consistent with those obtained from Eq. (23).

Overall Ca^{2+}-binding to sites B on the vesicle and to the complex DB

Similar to the overall reaction scheme (16) for DNA-binding, we express the overall binding according to:

$$Ca + (B + DB) \rightleftharpoons (CaB + DCaB(DCa)) \tag{26}$$

where the DNA-dependent overall equilibrium constant is defined by:

$$\overline{K'^{(D)}_{Ca}} = [Ca] \cdot \frac{[B] + [DB]}{[CaB] + [DCaB(DCa)]} = [Ca] \cdot \frac{1 - \overline{\beta_{Ca}}}{\overline{\beta_{Ca}}} = [Ca]_{\overline{\beta_{Ca}} = 0.5}. \tag{27}$$

The overall degree of Ca^{2+}-binding refers to:

$$\overline{\beta_{Ca}} = \frac{[CaB] + [DCaB(DCa)]}{([CaB] + [DCaB(DCa)])^{max}} = \frac{[Ca_b]}{[Ca_b(D)]^{max}} = \frac{[Ca]}{[Ca] + \overline{K'^{(D)}_{Ca}}}. \tag{28}$$

The part (DCa) in the complex DCaB(DCa) accounts for the Ca^{2+}-binding to those base pairs of DNA which are not yet bridged by Ca^{2+}-ions to the lipid surface. Consistent with expectations, the concentration of bound Ca^{2+} in the pellet $[Ca_b]$ = [CaB] + [DCaB(DCa)] increases with increasing $[Ca_t]$ and $[D_t]$, respectively (Fig. 10). Trivially at [D] = 0, $[Ca_b]$ = [CaB]. With increasing $[D_t]$, $[Ca_b]$ in the complex [DCaB(DCa)] increases first due to Ca^{2+}-bridging D and B as complex DCaB and then additionally due to further Ca^{2+}-binding to the DNA (as DCa) not yet bridged to B-sites as DCaB, reducing the amount of CaB.

Parallel to the formalism used for the overall DNA-binding, the overall equilibrium constant $\overline{K'^{(D)}_{Ca}}$ for the Ca^{2+}-binding is given by:

$$\overline{K'^{(D)}_{Ca}} = K'_{Ca} \cdot \frac{[D] + K^0_D}{[D] + K'_D}, \tag{29}$$

Eq. (29) is derived from Eq. (27); see Eq. (A5) of the appendix. From Eq. (28) we obtain the double–reciprocal relationship:

$$\frac{1}{[Ca_b]} = \frac{1}{[Ca_b(D)]^{max}}\left(1 + \overline{K'_{Ca}}^{(D)} \frac{1}{[Ca]}\right). \qquad (30)$$

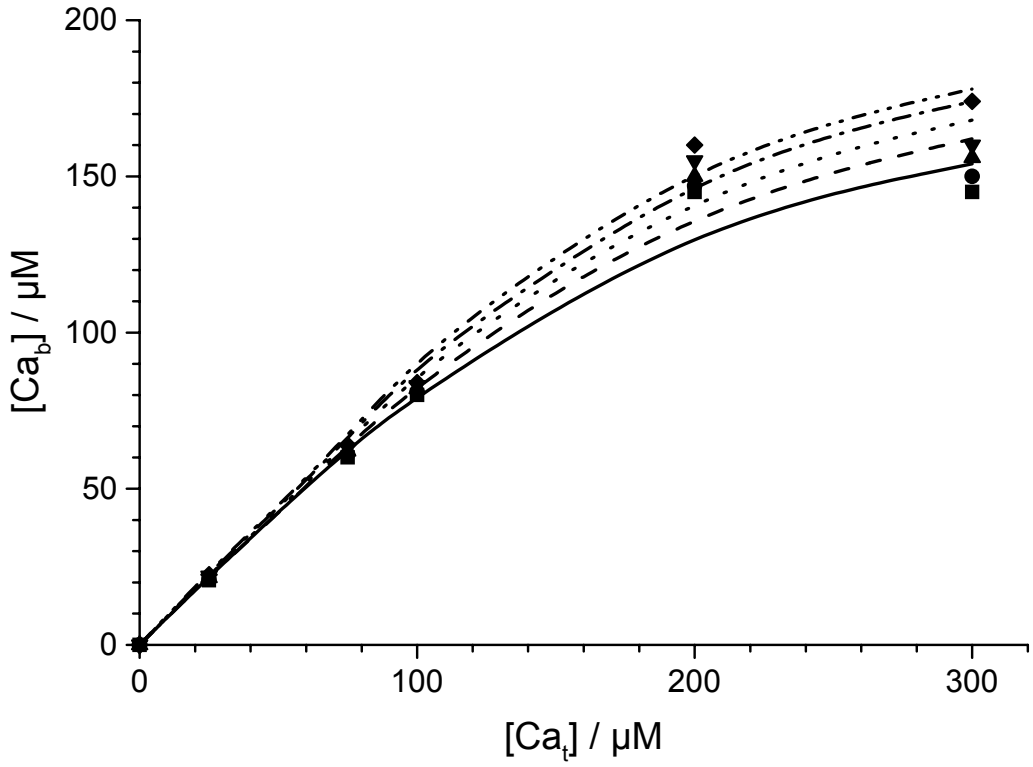

Fig. 10 The concentration $[Ca_b] = [CaB] + [DCaB(DCa)] = [Ca_t] - [Ca_t]^{sup}$ of bound Ca^{2+} in the pellet for $[D_t]$ / µM (bp) = (■) 0, (●) 35.5, (▲) 71, (▼) 107 and (◆) 143 versus $[Ca_t]$. Note, that $[D_t]$ refers to the concentration of DNA in the vesicle suspension.

Using Eq. (30) at different $[D_t]$, the intercepts yield $[Ca_b(D)]^{max}$ and $\overline{K'_{Ca}}^{(D)}$, respectively (Fig. 11). For each $\overline{K'_{Ca}}^{(D)}$ at a given $[D_t]$ there is a half-point concentration $[Ca_b]_{0.5} = [Ca_b(D)]^{max}/2$ at given $[Ca_t]_{0.5}$, $[Ca]_{0.5}$ and $[D]_{0.5}$, respectively. It is seen that the values of $\overline{K'_{Ca}}^{(D)}$ are equal to those of $[Ca]_{0.5}$, within the error margin. The coordinates of the intersection point are given by Eq. (A6) of the appendix.

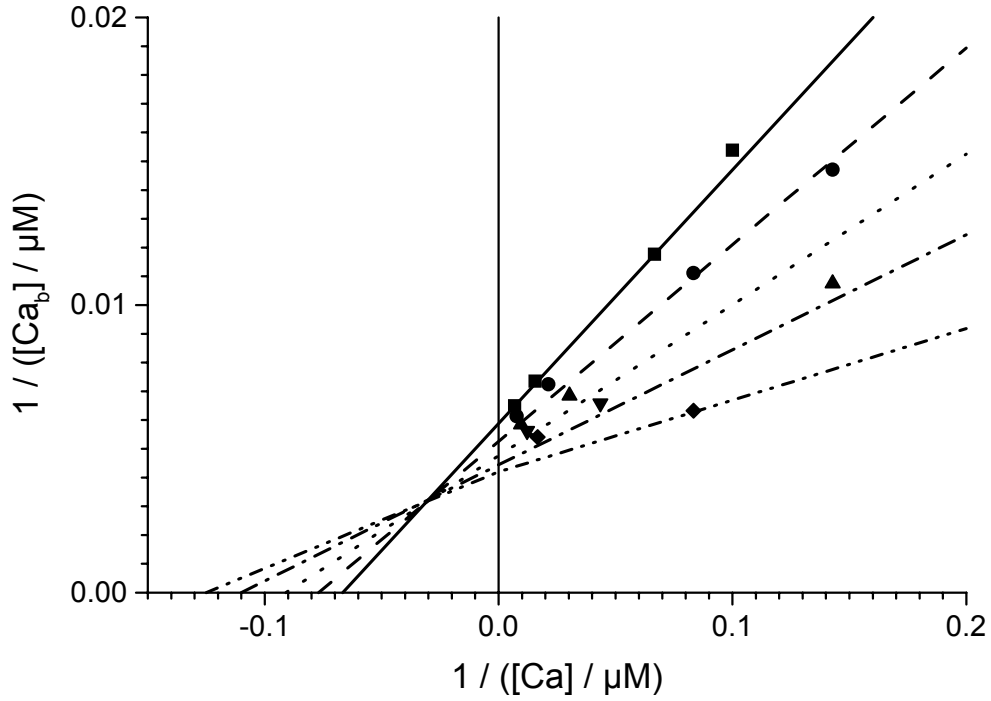

Fig. 11 Determination of $\overline{K'_{Ca}}^{(D)}$ and $[Ca_b]^{max}$ from the double-reciprocal relationship Eq. (30) for $[D_t]$ / μM (bp) = (■) 0, (●) 35.5, (▲) 71, (▼) 107 and (◆) 143. (The intersection point is at: $1/[Ca]_i$ = -0.03 μM^{-1} and $1/[Ca_b]_i$ = 0.0032 μM^{-1} (see the appendix)).

As seen in Fig. 12, the overall equilibrium constant $\overline{K'_{Ca}}^{(D)}$ decreases with increasing half-point concentration $[D]_{0.5}$ according to Eq. (29) with $K_D^0 \gg K'_D$. At [D] = 0, $\overline{K'_{Ca}}^{(D)} = K_D^0 \cdot K'_{Ca} / K'_D = K_{Ca}^0$ and at $[D] \gg [D_t]$ (saturation) we obtain $\overline{K'_{Ca}}^{(D)} = K'_{Ca}$. The data fit with Eq. (29) yields $K_{Ca}^0 = 15 \pm 5$ μM and $K'_{Ca} = 0.75 \pm 0.25$ μM at T = 293 K (20^0C), 1 mM HEPES, pH 7.4, confirming that indeed $K_{Ca}^0 \gg K'_{Ca}$.

The maximum concentration $[Ca_b(D)]^{max}$ of Ca^{2+} bound to the outer vesicle surface in the presence of bound DNA increases with increasing total concentration of DNA according to mass conservation:

$$[Ca_b(D)]^{max} = [CaB]^{min} + [DCaB(DCa)]^{max} = [CaB]^{max} + [D_t] - [DCaB]. \quad (31)$$

Note that $[DCaB]^{max} + [DCa]^{max} = [D_t]$ and $[CaB]^{min} = [CaB]^{max} - [DCaB]$. See the Fig. 6A of the appendix.

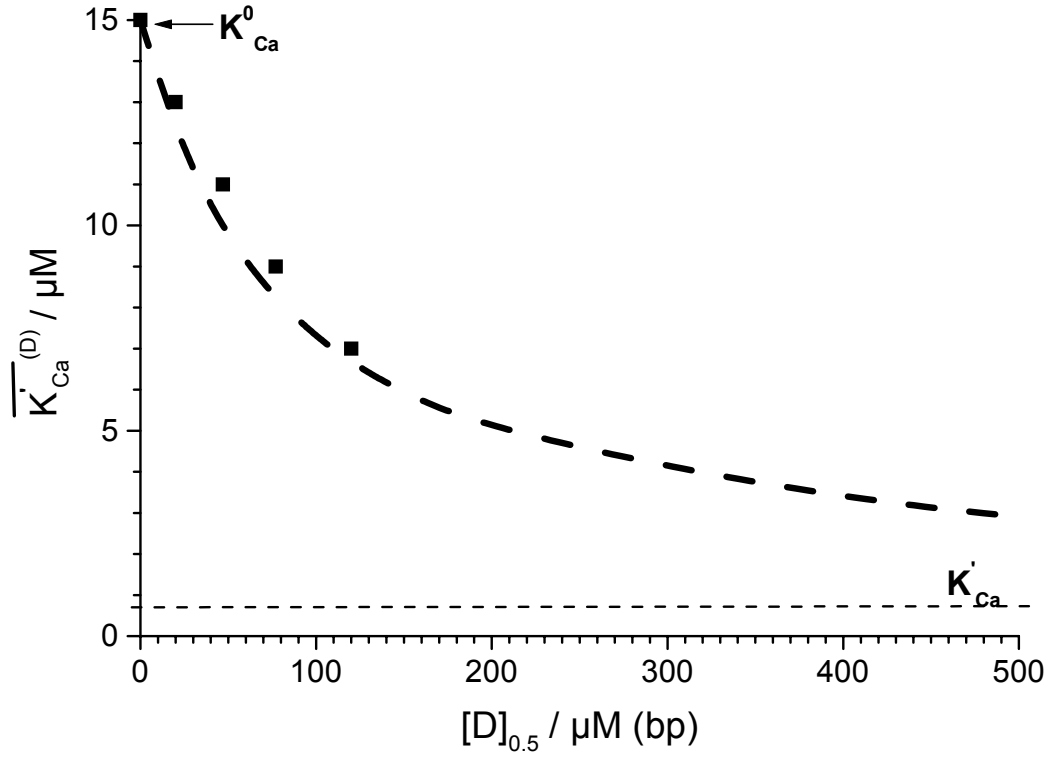

Fig. 12 The overall equilibrium constants $\overline{K'^{(D)}_{Ca}}$ determined with Eq. (30). Data fit with Eq. (29) yields $K^0_{Ca} = 15 \pm 5$ µM and $K'_{Ca} = 0.75 \pm 0.25$ µM at T = 293 K (20^0 C), 1 mM HEPES, pH 7.4.

As a further consistency check, $\overline{K'^{(D)}_{Ca}}$ is calculated using the values for [D], $[Ca_t]^{sup}$, $[Ca_b]$ and $[Ca_b(D)]^{max}$. Introducing Eq. (12) into Eq. (30) and rearranging yields:

$$\overline{K'^{(D)}_{Ca}} = \left(\frac{[Ca_b(D)]^{max}}{[Ca_b]} - 1\right) \cdot \frac{[Ca_t]^{sup} \cdot K^0_{CaD}}{[D] + K^0_{CaD}}. \qquad (32)$$

Data fit with Eq. (29) yields $K^0_{Ca} = 15 \pm 5$ µM and $K'_{Ca} = 0.75 \pm 0.25$ µM at T = 293 K (20^0C), 1 mM HEPES, pH 7.4. See the Fig. 7A of the appendix. These results are consistent with those obtained with Eq. (30).

The equilibrium constant K'_{CaD} is calculated using the definitions of the apparent equilibrium constants in Eqs. (7) and (8), respectively; according to:

$$K'_{CaD} = \frac{[CaD] \cdot [B]}{[DCaB]} = \frac{[D] \cdot [CaB]}{[DCaB]} \cdot \frac{[Ca] \cdot [B]/[CaB]}{[Ca] \cdot [D]/[CaD]} = K'_D \cdot \frac{K^0_{Ca}}{K^0_{CaD}}. \qquad (33)$$

Eq. (33) yields $K'_{CaD} = 53 \pm 10$ µM (bp) at T = 293 K (20^0 C), 1 mM HEPES, pH 7.4.

As seen in Tab. 2, the dissociation equilibrium constants for the binary complexes are greater as the respective constants for the ternary complexes, i.e. the ternary complexes are more stable than the binary complexes.

Tab. 2 The apparent dissociation equilibrium constants for the system DNA, Ca^{2+}-ions, lipid vesicle surface (PS) in 1 mM HEPES, pH 7.4, T = 293 K (20^0 C).

Binary complexes	Ternary complexes
$K^0_{Ca} = 15 \pm 5$ μM	$K'_{Ca} = 0.75 \pm 0.25$ μM
$K^0_{CaD} = 24 \pm 5$ μM	$K'_{CaD} = 53 \pm 10$ μM (bp)
$K^0_{D} = 1.7 \pm 0.1$ mM (bp)	$K'_{D} = 85 \pm 15$ μM (bp)

Conclusions

Using centrifugation, atom absorption spectrometry and arsenazo III absorbance, the binding of DNA at lipid vesicle surface mediated by Ca^{2+}-ions is measured. The independent spectroscopic measurements permit the determination of the apparent dissociation equilibrium constants for the binary complexes: Ca/lipid vesicles, Ca/DNA and DNA/lipid vesicles and for the various processes leading to the ternary complex DNA/Ca/lipid vesicles. The thermodynamic formalism has been developed such that the experimental overall dissociation equilibrium constants for the binding of Ca^{2+} and DNA to the vesicle surface, respectively, appear as combinations of the individual binary equilibrium constants. The thermodynamic stabilities of the respective ternary complexes are two orders of magnitude greater than that of the binary complexes: Ca/lipids and DNA/lipids.

The knowledge of the equilibrium constants for the adsorption of DNA and the binding of DNA to the vesicle surface, provide the basis for choosing the respective optimal concentrations, to optimize the conditions of the adsorption for the direct electrotransfer of gene-DNA into biological cells and tissue.

Acknowledgments

We gratefully acknowledge support of the Fonds Chemie, Frankfurt, the Ministry MSWF of the Land NRW for Grant Elminos, the European Union (Brüssel) for Grant QLK3-CT-1999-00484 and the Deutsche Forschungsgemeinschaft for Grants Ne227/9-3 and 9-4 to E.N.

Appendix

The binding of Ca^{2+} to DNA in the supernatant. In the presence of vesicles, the degree β_{CaD} of Ca^{2+} binding to DNA is given by:

$$\beta_{CaD} = \frac{[CaD]}{[CaD]^{max}} = \frac{[CaD]}{[D_t]^{sup}} = \frac{[Ca]}{[Ca] + K^0_{CaD}} \tag{A1}$$

where the relation $[D_t]^{sup} = [CaD]^{max}$ holds.

Note that $K^0_{CaD} = [Ca]\cdot[D]/[CaD] = [Ca]\cdot(1-\beta_{CaD})/\beta_{CaD}$; hence $\beta_{CaD}\cdot(K^0_{CaD} + [Ca]) = [Ca]$ yielding Eq. (A1) or the relationship: $[CaD] = [D_t]^{sup}\cdot[Ca]/([Ca] + K^0_{CaD})$. Insertion into $[Ca_t]^{sup} = [Ca] + [CaD]$ yields: $[Ca] = [Ca_t]^{sup} - [D_t]^{sup}\cdot[Ca]/([Ca] + K^0_{CaD})$.

The equilibrium constant $K^0_{CaD} = [Ca]_{\beta_{CaD} = 0.5}$ in the presence of vesicles is related to the total Ca^{2+} concentration $[Ca_t]^{sup}$ of supernatant and the total DNA concentration $[D_t]^{sup}$ in the supernatant by:

$$[Ca_t]^{sup}_{0.5} = K^0_{CaD} + [D_t]^{sup}/2. \tag{A2}$$

Determination of [Ca] with Ar. Similar to Eq. (A2), the equilibrium constant $K_{CaAr} = 3.5 \pm 0.5$ μM is obtained from the midpoint (half-point) of the relation ΔA_{602} vs. log ($[Ca_t]$/mM) (data not shown) according to:

$$K_{CaAr} = [Ca_t]_{\beta_{CaAr} = 0.5} - [Ar_t]/2, \tag{A3}$$

where $[Ca_t]_{\beta_{CaAr} = 0.5}$ refers to $\Delta A_{602} = \Delta A^{max}_{602}/2$ and $\Delta A_{602} = A_{602} - A^0{}_{602}$ and $A^0{}_{602} = \varepsilon_{Ar}\cdot d\cdot[Ar_t]$ at [Ca] = 0 (experimentally realised with 1 mM EDTA).

Overall DNA-binding to sites B on the vesicle and to complex CaB. Using the definitions of the apparent equilibrium dissociation constants in Eqs. (7) and (8), respectively, of the main text, the overall equilibrium constant for the Ca^{2+}-dependent binding of DNA is defined as:

$$\begin{aligned}\overline{K'_D}^{(Ca)} &= [D]\cdot\frac{[B]+[CaB]}{[DB]+[DCaB]} = [D]\cdot\frac{[B]\cdot(1+[CaB]/[B])}{[DB]\cdot(1+[DCaB]/[DB])} \\ &= K^0_D\cdot\frac{1+[Ca]/K^0_{Ca}}{1+[Ca]/K'_{Ca}} = K^0_D\cdot\frac{K'_{Ca}}{K^0_{Ca}}\cdot\frac{[Ca]+K^0_{Ca}}{[Ca]+K'_{Ca}} = K'_D\cdot\frac{[Ca]+K^0_{Ca}}{[Ca]+K'_{Ca}}\end{aligned} \tag{A4}$$

where the relation $K^0_D/K^0_{Ca} = K'_D/K'_{Ca}$ of the cyclic scheme (Fig. 7) is used. See Eq. (20) of the main text.

Overall Ca^{2+}-binding to sites B on the vesicle and to complex DB. The overall equilibrium constant for the DNA-dependent binding of Ca^{2+} according to scheme (26) is given by:

$$\begin{aligned}\overline{K'_{Ca}}^{(D)} &= [Ca]\cdot\frac{[B]+[DB]}{[CaB]+[DCaB(DCa)]}\\ &= [Ca]\cdot\frac{[DB]\cdot(1+[B]/[DB])}{[DCaB(DCa)]\cdot(1+[CaB]/[DCaB(DCa)])}\\ &= K'_{Ca}\cdot\frac{1+K^0_D/[D]}{1+K'_D/[D]} = K'_{Ca}\cdot\frac{[D]+K^0_D}{[D]+K'_D}\end{aligned} \qquad \text{(A5)}$$

where the relation $K'_{Ca} = K'_D\cdot K^0_{Ca}/K^0_D$ is inherent; see Eq. (29) of the main text.

The intersection point in Fig. 11 is obtained from Eq. (30) of the main text for $[D_t] \neq 0$ and $[D_t] = 0$, where $1/[Ca_b] = (1/[Ca_b]^{max})(1+K^0_{Ca}/[Ca])$. The coordinates $1/[Ca]_i$ and $1/[Ca_b]_i$ of the intersection point are given by:

$$\begin{aligned}\frac{1}{[Ca]_i} &= -\frac{[Ca_b(D)]^{max}-[Ca_b]^{max}}{[Ca_b(D)]^{max}\cdot K^0_{Ca}-[Ca_b]^{max}\cdot\overline{K'_D}^{(D)}}\\ \frac{1}{[Ca_b]_i} &= \frac{K^0_{Ca}-\overline{K'_{Ca}}^{(D)}}{[Ca_b(D)]^{max}\cdot K^0_{Ca}-[Ca_b]^{max}\cdot\overline{K'_{Ca}}^{(D)}}\end{aligned} \qquad \text{(A6)}$$

In Fig. 11, we see that $[Ca]_i = -0.03\ \mu M^{-1}$ and $[Ca_b]_i = 0.0032\ \mu M^{-1}$.

Additional explanatory figures

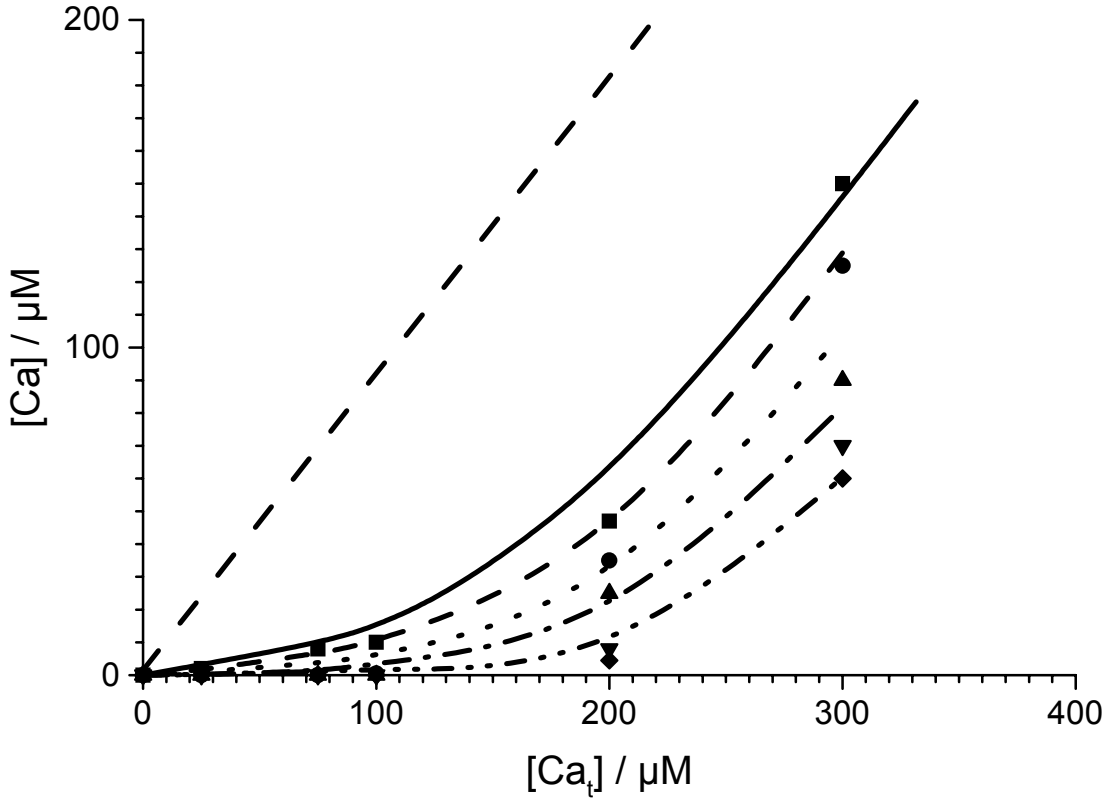

Fig. 1A Ca^{2+}-binding isotherms for different DNA concentrations: $[D_t]$ / µM (bp): (■) 0, (●) 35.5, (▲) 71, (▼) 107 and (◆) 143; from top to bottom. The data are fitted with Eq. (12) of the text, where $[Ca_t] = [Ca_b] + [Ca_t]^{sup}$. The straight dashed line represents the case without vesicles and without DNA for which $[Ca] = [Ca_t] = [Ca_t]^{sup}$.

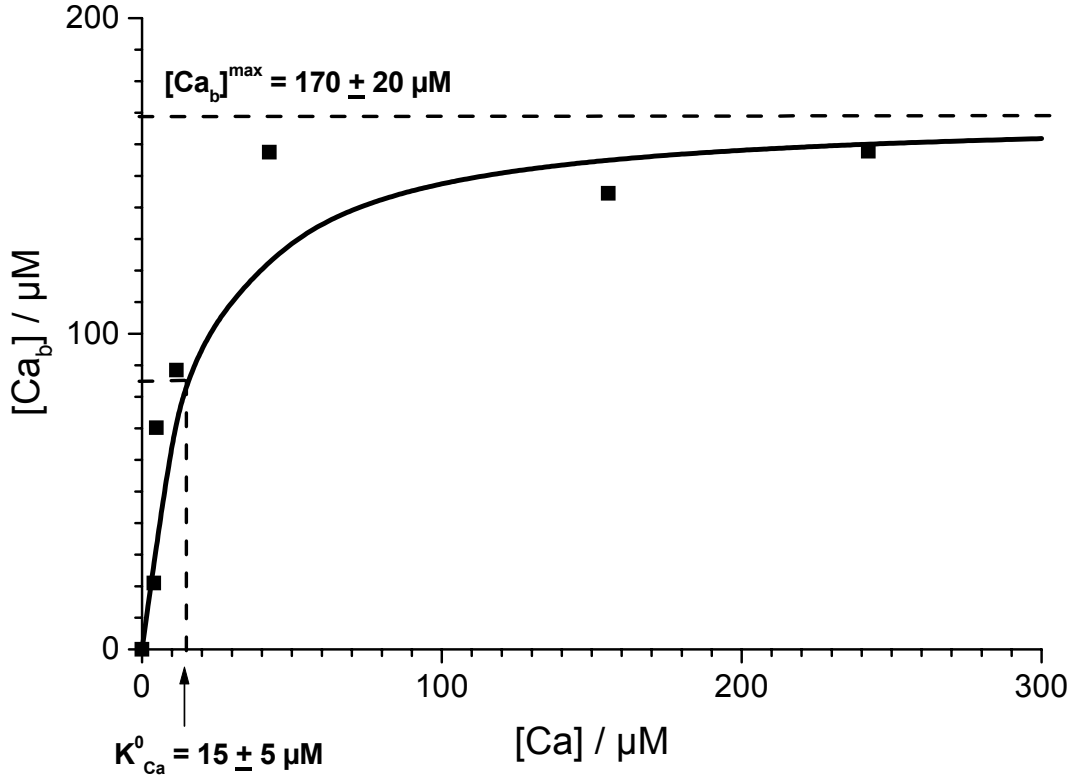

Fig. 2A Ca^{2+}-binding isotherms in the absence of DNA, $[Ca_b] = [Ca_t] - [Ca]$, in the pellet as a function of [Ca] in the supernatant. The data points represent mean values of two measurements Ca^{2+} in the supernatant by arsenazo III–absorption and atomic absorption spectroscopy. Here, $[Ca] = [Ca_t]^{sup}$. Data fit with Eq. (10) of the text yields the equilibrium constant $K^0_{Ca} = 15 \pm 5$ µM and $[Ca_b]^{max} = 170 \pm 20$ µM at T = 293 K (20^0 C), 1 mM HEPES, pH 7.4.

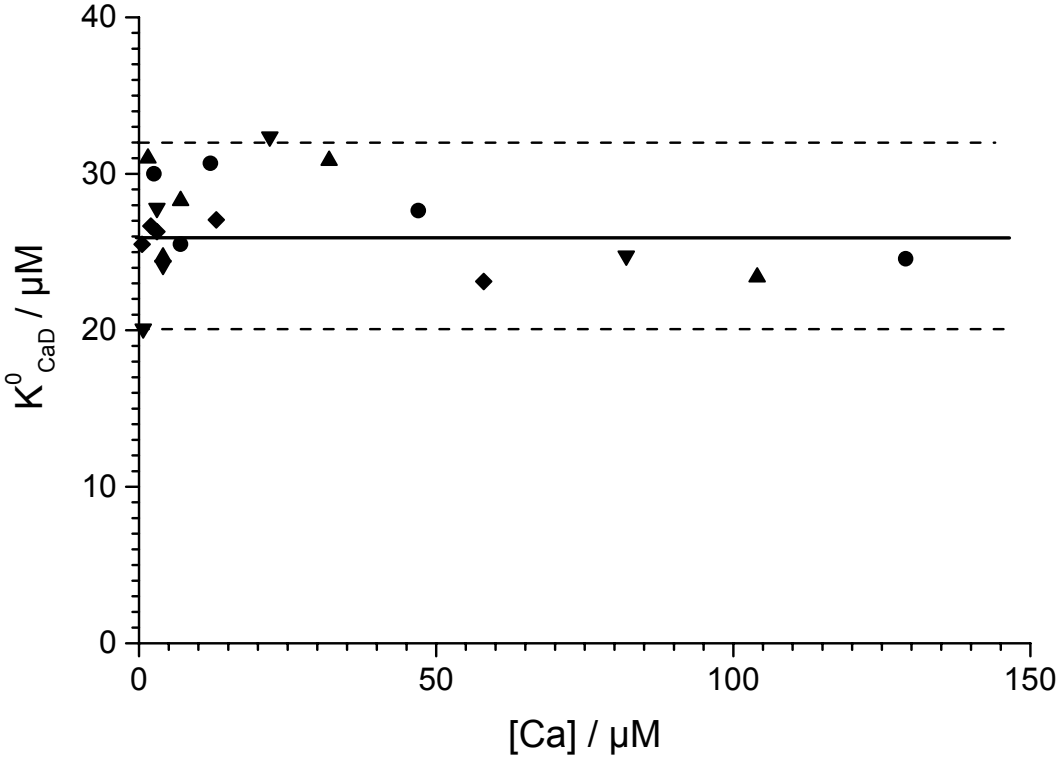

Fig. 3A The equilibrium constant K^0_{CaD} calculated with Eq. (15) for $[D_t]$ / µM (bp) = (●) 35.5, (▲) 71, (▼) 107 and (◆) 143 as a function of [Ca]. The straight thick line represents the mean of $K^0_{CaD} = 26 \pm 6$ µM.

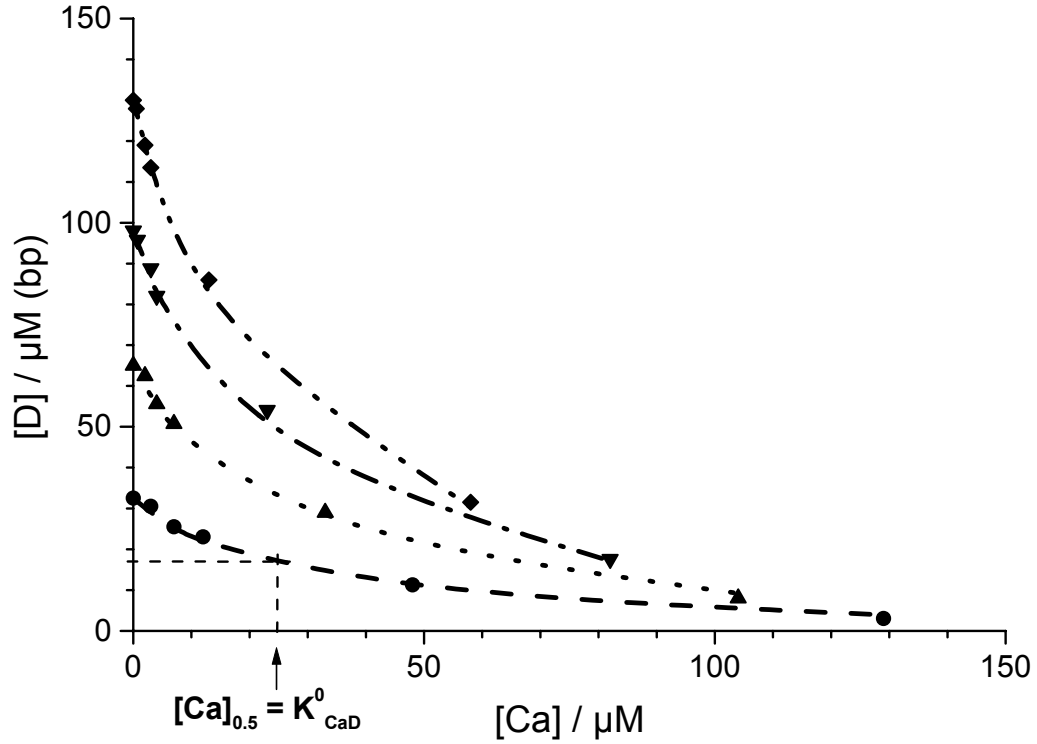

Fig. 4A The relationship between $[D] = [Ca] + [D_t]^{sup} - [Ca_t]^{sup}$ and [Ca] for $[D_t]$ / µM (bp) = (●) 35.5, (▲) 71, (▼) 107 and (◆) 143. $[D_t]$ refers to the concentration of DNA in the vesicle suspension. The data are fitted with the Eq. (19) of the text.

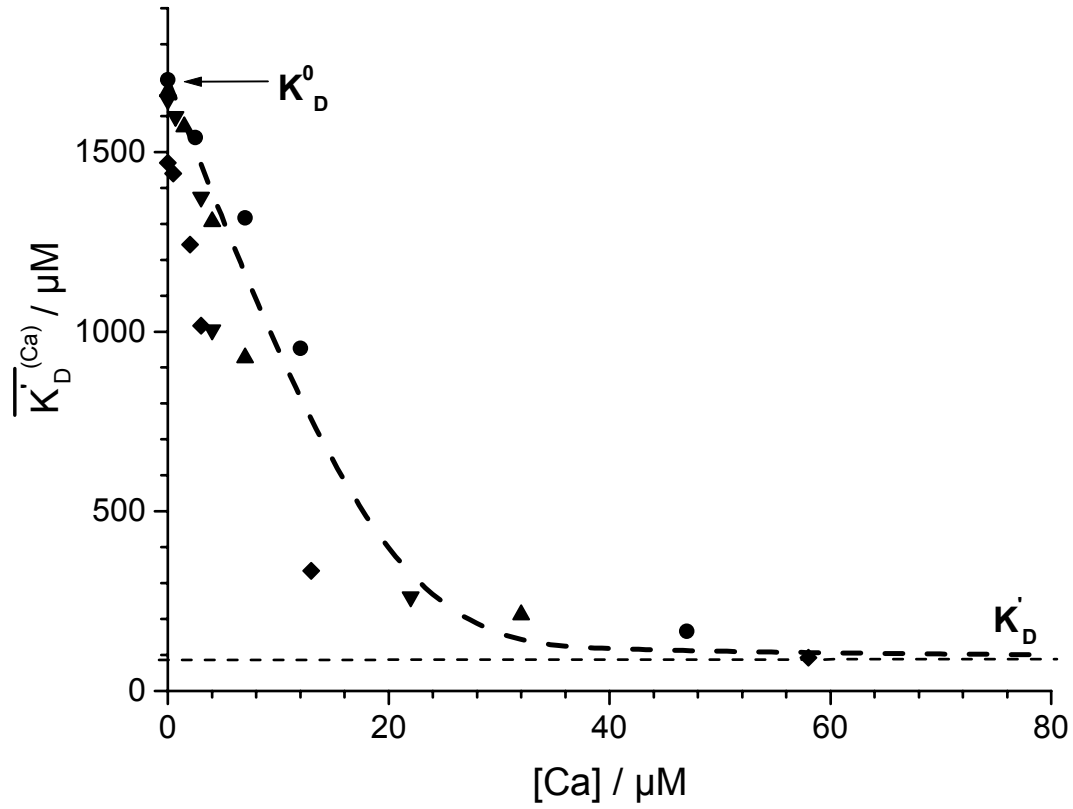

Fig. 5A The overall binding constant $\overline{K'^{(Ca)}_D}$ calculated with Eq. (25) for $[D_t]$ / µM (bp) = (●) 35.5, (▲) 71, (▼) 107 and (◆) 143 as a function of [Ca]. $[D_t]$ refers to the total concentration of DNA in the vesicle suspensions. The data fit with Eq. (20) yields K'_D = 85 ± 15 µM (bp) and K^0_D = 1.7 ± 0.1 mM (bp) at T = 293 K (20^0 C), 1 mM HEPES, pH 7.4.

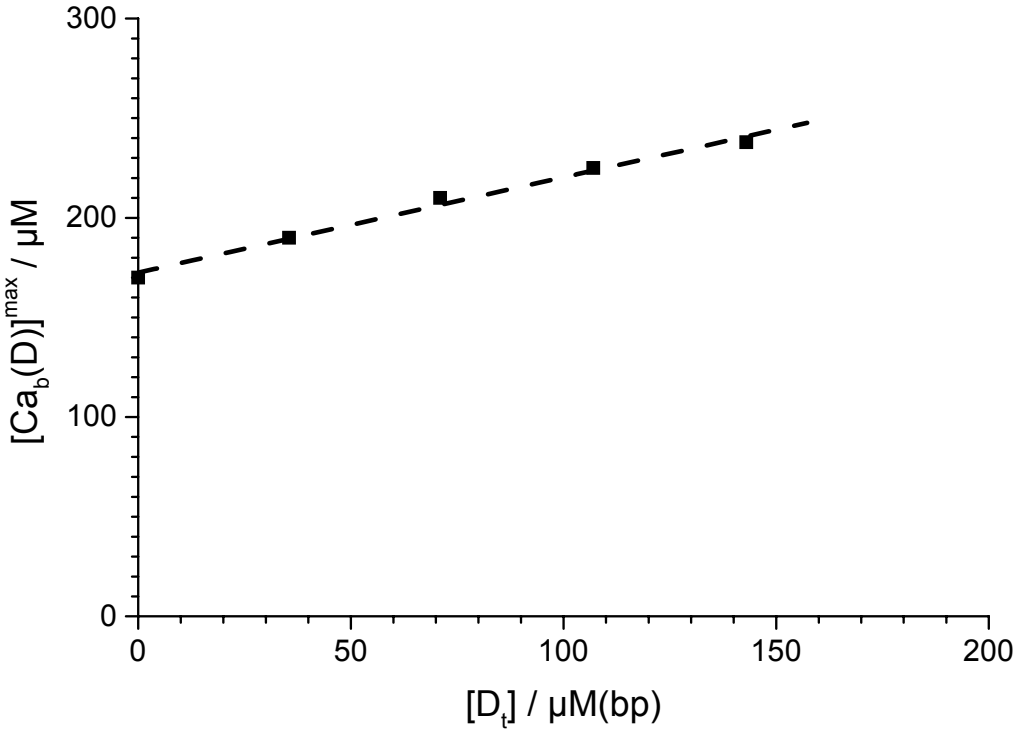

Fig. 6A The total concentrations of sites available for Ca^{2+}-binding on the vesicle surface $[Ca_b(D)]^{max}$ = $[CaB]^{max}$ + $[D_t]$ – [DCaB]. $[Ca_b(D)]^{max}$ increases linearly with $[D_t]$ due to the increased number of sites D(bp) not involved in the ternary complex DCaB, but binding Ca^{2+}-ions as CaD within the DNA partially attached to the lipid surface.

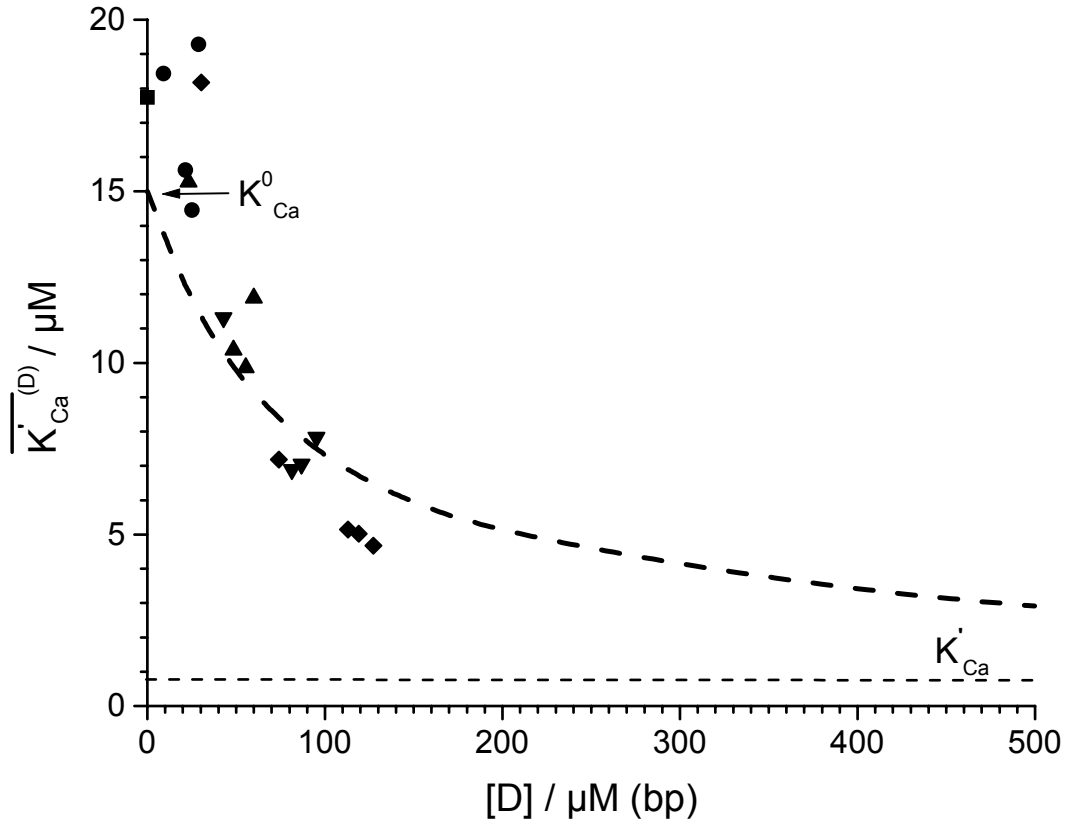

Fig. 7A The overall equilibrium constants $\overline{K'_{Ca}}^{(D)}$ as a function of [D] calculated with Eq. (32) of the text for $[D_t]$ / μM (bp) = (■) 0, (●) 35.5, (▲) 71, (▼) 107 and (◆) 143. Data fit with Eq. (29) yields $K^0_{Ca} = 15 \pm 5$ μM and $K'_{Ca} = 0.75 \pm 0.25$ μM at T = 293 K (20^0 C), 1 mM HEPES, pH 7.4.

Reference List:

[1] L.M. Mir, M.F. Bureau, J. Gehl, R. Rangara, D. Rouy, J.-M. Caillaud, P. Delaere, D. Branellec, B. Schwartz, D. Scherman, High-efficiency gene transfer into skeletal muscle mediated by electric pulses, Proc. Natl. Acad. Sci. USA 96 (1999) 4262-4267.

[2] E. Neumann, M. Schaefer-Ridder, Y. Wang, P.H. Hofschneider, Gene transfer into mouse lyoma cells by electroporation in high electric fields, EMBO J. 1 (1982) 841-845.

[3] U. Pliquett, R. Elez, A. Piiper, E. Neumann, Electroporation of subcutaneous mouse tumors by rectangular and trapezium high voltage pulses, Biolectrochem. 62 (2004) 83-93.

[4] L.M. Mir, S. Orlowski, J. Belehradek Jr., J. Teissie, M.P. Rols, G. Sersa, D. Miklavcic, R. Gilbert, R. Heller, Biomedical applications of electric pulses with special emphasis on antitumor electrochemotherapy, Bioelectrochem. Bioenerg. 38 (1995) 203-207.

[5] R. Elez, A. Piiper, B. Kronenberger, M. Kock, M. Brendel, E. Hermann, U. Pliquett, E. Neumann, S. Zeuzem, Tumor regression by combination antisense therapy against Plk1 and Bcl-2, Oncogene 22 (2003) 69-80.

[6] C. Newton, W. Pangborn, S. Nir, D. Papahadjopoulos, Specificity of Ca^{2+} and Mg^{2+} binding to phosphatidylserine vesicles and resultant phase changes of bilayer membrane structure, Biochim. Biophys. Acta 506 (1978) 281-287.

[7] A. Portis, C. Newton, W. Pangborn, D. Papahadjopoulos, Studies of the mechanism of membrane fusion: evidence for an intermembrane Ca^{2+}-phospholipid complex, synergism with Mg^{2+}, and inhibition by spectrin, Biochem. 18 (1979) 780-790.

[8] S. McLaughlin, N. Murline, T. Gresalfi, G. Vaio, A. McLaughlin, Adsorption of divalent cations to bilayer membranes containing phosphatidyserine, J. Gen. Physiol. 77 (1981) 445-473.

[9] J. Bentz, S. Nir, Cation Binding to Membranes: Competition between mono-, di- and trivalent cations, Bull. Math. Biol. 42 (1980) 191-220.

[10] A.M.I. Lam, P.R. Cullis, Calcium enhances the transfection potency of plasmid DNA-cationic liposome complexes, Biochim. Biophys. Acta, 1463 (2000) 279-290.

[11] D.P. Kharakoz, R.S. Khusainova, A.V. Gorelov, K.A. Dowson, Stoichiometry of dipalmitoylphosphatidylcholine-DNA interaction in the presence of Ca^{2+}: a temperature-scanning ultrasonic study, FEBS Lett. 446 (1999) 27-29.

[12] J.T. Shapiro, B.S. Stannard, G. Felsenfeld, The binding of small cations to deoxyribonucleic acid. nucleotide specificity, Biochem. 8 (1969) 3233-3241.

[13] L. Jin, P. Yang, Synthesis and DNA-binding studies of a nickel(II) coordination compound, Microchem. J. 58 (1998) 144-150.

[14] N. Korolev, A.P. Lyubartsev, A. Ruprecht, L. Nordenskiöld, Competitive binding of Mg^{2+}, Ca^{2+}, Na^{+} and K^{+} Ions to DNA in oriented DNA fibers: experimental and Monte Carlo simulation results, Biophys. J. 77 (1999) 2736-2749.

[15] E. Süleymanoglu, A Nanoscale Polynucleotide-neutral liposome self-assemblies formulated for therapeutic gene delivery, Electronic J. Biomed. 2(2) (2004).

[16] E. Neumann, S. Kakorin, I. Tsoneva, B. Nikolova, T. Tomov, Calcium-mediated DNA adsorption to Yeast cells and kinetics of cell transformation by electroporation, Biophys. J. 71 (1996) 868-877.

[17] N. Stoicheva, I. Tsoneva, D.S. Dimitrov, I. Panaiotov, Kinetics of calcium-induced fusion of cell-size liposomes with monolayers in solutions of different osmolarity, Z. Naturforsch. 40c (1985) 92-96.

[18] F. Olson, C.A. Hunt, F.C. Szoka, W.J. Vail, D. Papahadjopoulos, Preparation of liposomes of defined size distribution by extrusion through polycarbonate membranes, Biochim. Biophys. Acta 557 (1979) 9-23.

[19] L.D. Mayer, M.J. Hope, P.R. Cullis, Vesicles of variable sizes produced by a rapid extrusion procedure, Biochim. Biophys. Acta 858 (1986) 161-168.

[20] P. L. Dorogi, E. Neumann, Spectrophotometric Determination of reaction stoichiometry and equilibrium constants of metallochromic indicators. II. The Ca^{2+}-arsenazo III complexes, Biophys. Chem. 13 (1981) 125-131.

[21] V. Michaylova, P. Ilkova, Photometric determination of micro amounts of calcium with arsenazo III, Anal. Chim. Acta 53 (1971) 194-198.

[22] P.L. Dorogi, C.R. Rabl, E. Neumann, Kinetic scheme for Ca^{2+}-arsenazo III interactions, Biochem. Biophys. Res. Commun. 111 (1983) 1027-1033.

[23] J.B. Willis, Determination of calcium and magnesium in urine by atomic absorption spectroscopy, Anal. Chem. 33 (1961) 556-559.

[24] D.J. Volsky, A. Loyter, Role of Ca^{2+} in Virus-induced membrane fusion. Ca^{2+} accumulation and ultrastructural changes induced by *Sendai* virus in chicken erythrocytes, J. Cell Biol. 78 (1978) 465-479.

[25] D. Huster, K. Arnold, K. Gawrisch, Strength of Ca^{2+} binding to retinal lipid membranes: consequences for lipid organization, Biophys. J. 78 (2000) 3011-3018.

[26] C. Mangavel, R. Maget-Dana, P. Tauc, J.-C. Brochon, D. Sy, J.A. Reynaud, Structural investigations of basic amphipathic model peptides in the presence of lipid vesicles

studied by circular dichroism, fluorescence, monolayer and modeling, Biochim. Biophys. Acta 1371 (1998) 265-283.

[27] T. Seimiya, S. Ohki, Ionic structure of phospholipid membranes, and binding of calcium ions, Biochim. Biophys. Acta 298 (1973) 546-561.

[28] S. Nir, C. Newton, D. Papahadjopoulos, Binding of cations to phosphatidylserine vesicles, Bioelectrochem. Bioenerg. 5 (1978) 116-133.

[29] H. Hauser, D. Chapman, R.M.C. Dawson, Physical Studies of Phospholipids. XI. Ca^{2+} binding to monolayers of phosphatidylserine and phosphatidylinositol, Biochim. Biophys. Acta 183 (1969) 320-333.

[30] P.G. Barton, The Influence of surface charge density of phosphatides on the binding of some cations, J. Biol. Chem. 243 (1968) 3884-3890.

[31] C. Xu, L.M. Loew, The effect of asymmetric surface potentials on the intramembrane electric field measured with voltage-sensitive dyes, Biophys. J. 84 (2003) 2768-2780.

[32] C. Fleck, R.R. Netz, H.H. von Grünberg, Poisson-Boltzmann theory for membranes with charged lipids and the pH-dependent interaction of a DNA molecule with a membrane, Biophys. J. 82 (2002) 76-92.

Glossary

Ar	arsenazo III
a_{coll}	collapse area per molecule
B	binding sites on the outside vesicle surface
β_{Ca}, β_{CaAr}, β_{CaD}	degree of Ca^{2+}-binding to vesicle surface, arsenazo III and DNA, respectively
$[Ca_t]$, $[D_t]$	total concentrations of Ca^{2+} and DNA, respectively
[Ca], [D]	free concentrations of Ca^{2+} and DNA in the supernatant, respectively
$[Ca_t]^{sup}$, $[D_t]^{sup}$	total concentrations of Ca^{2+} and DNA in the supernatant, respectively
$[Ca_b]$, $[D_b]$	concentrations of bound Ca^{2+} and bound DNA in the pellet, respectively
$[Ca_b(D)]^{max}$	maximum concentration of sites available for Ca^{2+}-binding on the vesicle surface, including the bound DNA
$[D_b]^0$	concentration of DNA bound to the vesicle surface at $[Ca_t] = 0$
K^0_{Ca}, K^0_D, K^0_{CaD}	dissociation equilibrium constants for the binary complexes
K'_{Ca}, K'_D, K'_{CaD}	dissociation equilibrium constants for the respective ternary complexe formations
$\overline{K'_{Ca}}^{(D)}$, $\overline{K'_D}^{(Ca)}$	overall dissociation equilibrium constants for the respective Ca^{2+}- and DNA binding
PS	phosphatidylserine
POPC	palmitoyl-oleoyl-phosphatidylcholine
PA	phosphoric acid
VET	vesicle extrusion technique

III. Eingereichtes Manuskript: submitted to Physical Chemistry Chemical Physics

Adsorption of DNA and electric fields decrease the rigidity of lipid vesicle membranes

*Alina Frantescu, Sergej Kakorin, Katja Toensing and Eberhard Neumann**

Physical and Biophysical Chemistry, Faculty of Chemistry, University of Bielefeld, Germany

Running title: DNA adsorption affects bilayer elasticity

Key words: lipid bilayer elasticity; turbidity dichroisms; vesicle electro-deformation; electroporation

* Correspondence to: Prof. Dr. Eberhard Neumann, Physical and Biophysical Chemistry, Faculty of Chemistry, University of Bielefeld, P. O. Box 100 131,

D-33501 Bielefeld, Germany. Phone: +49 521 106 20 53; Fax: +49 521 106 29 81

Abstract

The adsorption of calf–thymus DNA-fragments (300 ± 50 bp) in the total concentration range $0 \le [D_t] / \mu M\,(bp) \le 142$ to the membranes of unilamellar lipid vesicles is enhanced by Ca^{2+} ions (total Ca^{2+} concentration $[Ca_t] \le 1$ mM). The vesicles of radius a = 150 ± 45 nm are prepared from bovine brain extract type III containing 80-85% phosphatidylserine (PS) and palmitoyl-oleoyl-phosphatidylcholine (POPC) in the molar ratio PS:2POPC; total lipid concentration $[L_t]$ = 1 mM in 1 mM HEPES buffer, pH 7.4 at T = 293 K (20°C). The turbidity relaxations of the vesicle suspension at the wavelength λ = 365 nm in the electric fields E / (kV/cm) = 30, 40 and the pulse duration t_E = 10 μs indicate that the electroelongations of the vesicles are coupled to smoothing of membrane thermal undulations, membrane stretching and, at higher fields, to membrane electroporation. The quantitative analysis of the elongation kinetics suggests that the DNA adsorption to the vesicle surface (as ternary DNA/Ca/lipid complexes) renders the membrane more flexible and prone for potential electroporation. For instance, at E = 30 kV/cm and $[Ca_t]$ = 0.25 mM, membrane-bound DNA in the range $0 \le [D_b] / \mu M(bp) \le 40$, i.e., $0 \le N_b \le 118$ DNA fragments per one vesicle, decreases both the bending rigidity in the range $17 \ge \kappa / (10^{-20} J) \ge 13$ and the stretching modulus in the range $1.2 \ge K / (N/m) \ge 0.83$, respectively.

Introduction

The membrane electroporation (ME) technique[1,2] is widely used for introducing gene DNA and drugs, in particular chemotherapeutica, into isolated cells and tissue.[3-7] Traditionally, the lipid part of cell membranes is modelled with lipid bilayer vesicles[8,9] and many characteristic properties of lipid vesicles scale very well with those of biological cells.[10] The elastic properties of membrane, such as the spontaneous curvature and the bending rigidity, play an important role in the interactions of charged liposomes with colloidal nanoparticles and in the adsorption of neutral and ionic polymers to the outer surface of vesicle membranes.[11-13] It is known that the elastic properties and permeability of the lipid membrane can be altered not only by polymer adsorption and sugar asymmetry but also by electric fields.[12,14,15] For instance, prior adsorption of the anionic DNA on the outer surface of cells facilitates the electrotransfer of genes into the cell interior.[16] On the other hand, DNA-vesicle interactions have been studied intensively with positively charged vesicles,[17-21] but rarely with anionic liposomes.[22] The complexation of cationic liposomes with DNA can lead

to multilamellar complexes, vesicle aggregation or even vesicle rupture at higher DNA concentration.[23,24] To avoid vesicle aggregation, we have used small anionic unilamellar vesicles at low total lipid and Ca^{2+}-concentrations, respectively.[25] The Ca^{2+}-ions on the membrane surface are known to bridge the negatively charged DNA phosphate groups with the negatively charged lipid head groups of the vesicles.[16]

Further on, the application of electric pulses to vesicle suspensions can lead to smoothing of membrane undulations, membrane stretching, electroporation (ME) and to elongation of the vesicles at the expense of an increase in the projected membrane surface.[26] Here, the effect of the adsorption of DNA on the outer vesicle membrane surface is quantified using kinetic relaxation spectrometry in high electric field pulses.

Materials and Methods

Materials. Synthetic POPC (palmitoyl-oleoyl-phosphatidylcholine) from Lipoid GmbH (Ludwigshafen, Germany) and bovine brain extract type III (containing 80-85% PS) from Sigma Chemie GmbH (Deisenhofen, Germany) in the molar ratio PS:2POPC are used to prepare unilamellar vesicles of the average radius a = 150 ± 45 nm. The preparations of liposomes and of 300 ± 50 base pairs (bp) deoxyribonucleates by sonication of calf thymus (DNA type I, Sigma Chemie GmbH) are described elsewhere*. The total lipid concentration $[L_t]$ = 1 mM yields the vesicle number density $N_v = [L_t] / n_{ves} = 6.7 \cdot 10^{14} / L$, where $n_{ves} = 1.5 \cdot 10^{-18}$ mol is the content of lipids in one vesicle. The total calcium concentration $[Ca_t] \leq 1$ mM is far smaller than the limit for vesicle aggregation and fusion.[25] $[Ca_t]$ in the vesicles equals that in the bulk to avoid an osmotic pressure. The total concentration of DNA fragments in the vesicle suspension is in the range $0 \leq [D_t] / \mu M \text{ (bp)} \leq 142$.

Methods. In each case, one rectangular electric pulse with field strengths E = 30 or 40 $kVcm^{-1}$ and pulse duration of t_E = 10 µs has been applied to the vesicle suspension between the two planar graphite electrodes of the measuring chamber by cable discharge.[27] The sample cell is thermostated at T = 293 K (20° C). The sample chamber of about 1 ml is equipped with quartz windows with an optical path length of l = 1 cm. The field induced changes ΔOD_λ in the optical density $OD_\lambda = A_\lambda + T_\lambda$, where T_λ is the turbidity and A_λ the absorbance of plane-polarised light are measured at the wavelength λ = 365 nm (Hg-line). The light intensity change ΔI^σ, caused by electric pulse and measured at the two polarisation angles σ = 0, 90° relative to the applied external field E, is related to the optical density change by:

* Frantescu, A., Ph.D. Thesis, University of Bielefeld, 2005

$$\Delta OD^{\sigma} = OD^{\sigma}(E) - OD_0^{\sigma} = -\log(1 + \frac{\Delta I^{\sigma}}{I^{\sigma}}), \quad (1)$$

where $\Delta I^{\sigma} = I^{\sigma}(E) - I^{\sigma}$ is the intensity change from I^{σ} (at E = 0) to $I^{\sigma}(E)$ in the presence of E, and $OD^{\sigma}(E)$ and OD^{σ}_0 are the optical densities at E and at E = 0, respectively.

In the absence of an optical probe and outside the absorption band of the optical probe, the optical density OD is given solely by the turbidity T, hence OD = T. The field-induced change ΔT in T may be decomposed into a deformational/orientational part ΔT^{σ}_{OR} and a structural-chemical part ΔT^{σ}_{CH} according to $\Delta T^{\sigma} = \Delta T^{\sigma}_{OR} + \Delta T^{\sigma}_{CH}$.[28] The reduced turbidity minus mode is defined by:

$$\frac{\Delta T^{-}}{T_0} = \frac{\Delta T^{II} - \Delta T^{\perp}}{T_0} \quad (2)$$

where T_0 is the turbidity by E = 0 and $\Delta T^{II} = T^{II} - T_0$ and $\Delta T^{\perp} = T^{\perp} - T_0$ are the field induced changes at the two light polarisation modes $\sigma = 0°$ ($||$, parallel to the direction of external field) and $\sigma = 90°$ ($\perp$, perpendicular to the direction of external field), respectively. The reduced turbidity plus mode is analogous to the respective absorbance term[29] and given by:

$$\frac{\Delta T^{+}}{T_0} \equiv \frac{\Delta T_{CH}}{T_0} = \frac{\Delta T^{||} + 2\Delta T^{\perp}}{3T_0}. \quad (3)$$

It is recalled that the turbidity term $\Delta T^{-}/T_0$ contains also chemical contributions ΔT_{CH}, but refers primarily to global elongations of the vesicles in the electric field pulse. The term $\Delta T^{+}/T_0$ relates to chemical changes in the scattering cross section, for instance, due to entrance of water and ions in the membrane as well as to changes of the vesicle volume.

The refractive indices at different wavelengths in the visible range are determined using an Abbe-refractometer at T = 293 K (20^0 C) for different mole fractions x_{lip} of the lipids in the lipid/water system.[30] The values of the refractive indices at the wavelength λ = 365 nm are calculated using the Cauchy dispersion law. The refractive index $n_{lip} = 1.3639 \pm 0.0005$ of the pure lipid mixture PS:2POPC is obtained experimentally by the extrapolation of the refractive index of the mixture to $x_{lip} = 1$. The refractive index of the medium (buffer) is $n_{med} = 1.3483 \pm 0.0005$.

Results and data analysis

Turbidity relaxations. Since there is no vesicle aggregation, the initial optical density OD_0 at the field strength E = 0 and at the given $[Ca_t]$ slightly decreases with increasing total concentration $[D_t]$ of DNA (Fig. 1 a).

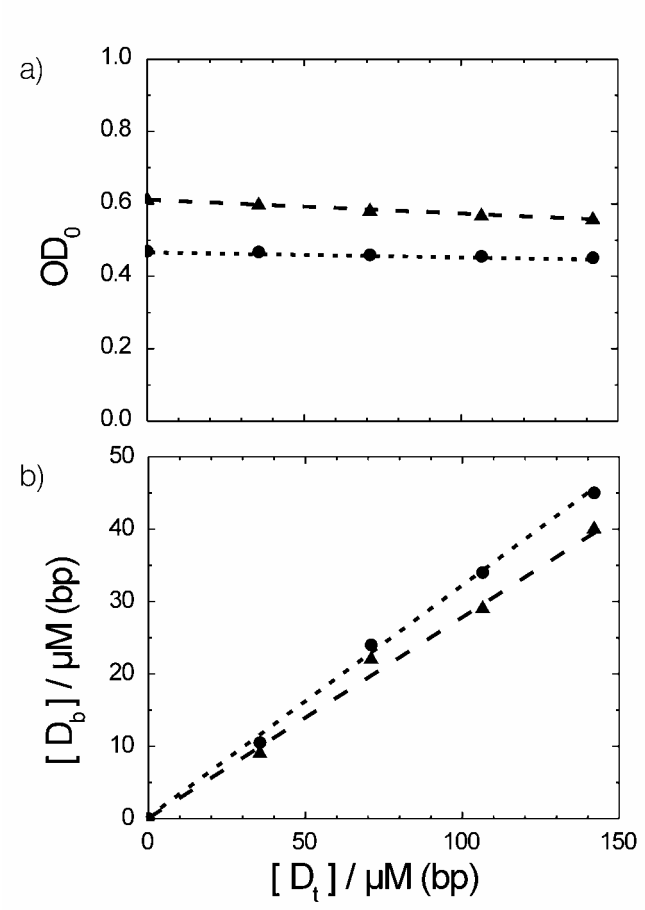

Fig. 1 Dependences on the total DNA concentration $[D_t]$ of: (a) the optical density OD_0 at the wavelength λ = 365 nm and at zero field strength, E = 0, of the suspension of unilamellar vesicles of radius a = 150 ± 45 nm; (b) the concentration $[D_b]$ of DNA fragments bound at the vesicle surface. The data points in (a) and (b) refer to the two total Ca^{2+} concentrations $[Ca_t]$ / mM = 0.25 (▲) and 0.75 (●) and the total lipid concentration $[L_t]$ = 1 mM, PS:2POPC in 1 mM HEPES, pH 7.4, T = 293 K (20 ^{0}C). The data in (a) suggest the absence of vesicle aggregation and vesicle fusion in the concentration range $0 \le [D_b]/\mu M(bp) \le 40$, i.e., $0 \le N_b \le 118$ DNA fragments per one vesicle.

Note that in the case of vesicle aggregation, OD_0 should steeply increase with $[D_t]$. The observed decrease in OD_0 can be rationalized by a decrease in the refractive index n_{lip} of the vesicle membrane caused by the adsorption of DNA in the membrane surface. Actually, the concentration $[D_b]$ of bound DNA linearly increases with increasing $[D_t]$ (Fig. 1 b).

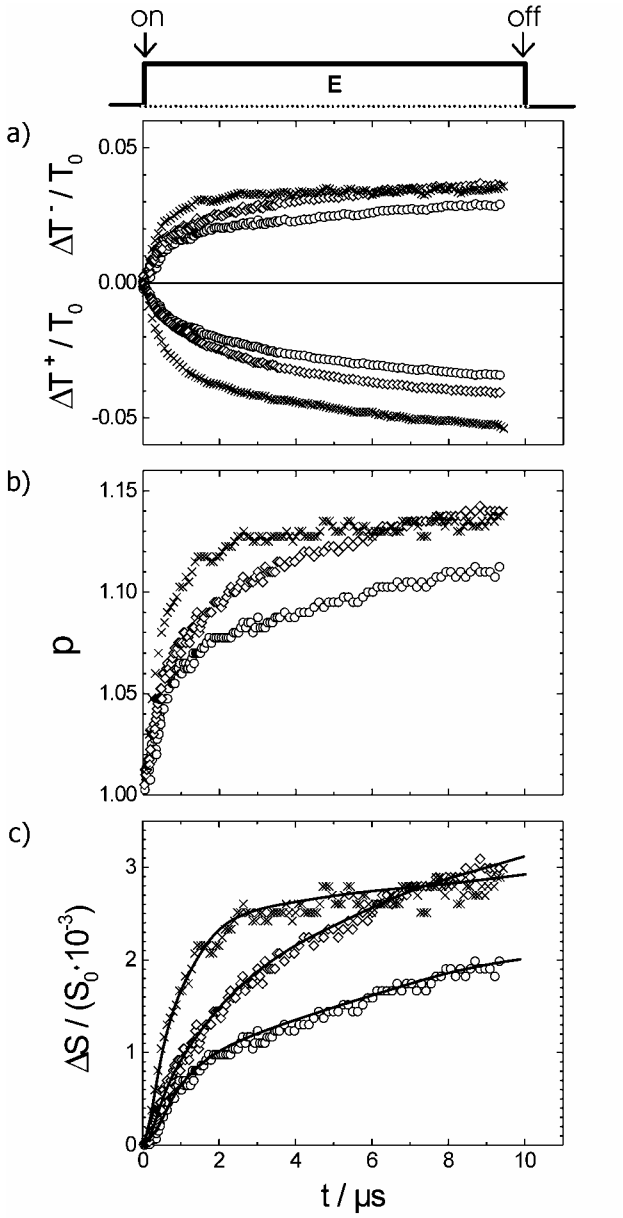

Fig. 2 High-field relaxation modes. (a) The dichroitic mode $\Delta T^{-}/T_0$ and the chemical mode $\Delta T^{+}/T_0$ at the wavelength λ = 365 nm and at the field strength E = 30 kV/cm, respectively; (x), $[Ca_t] = [D_t] = 0$; (○), $[Ca_t]$ = 0.25 mM and $[D_t] = 0$; (◇), $[Ca_t]$ = 0.25 mM and $[D_t]$ = 142 μM (bp). Other experimental conditions as in the legend to Fig. 1. (b) The axis ratio p = c/b of the electro-elongated vesicles, calculated from the $\Delta T^{-}/T_0$ and $\Delta T^{+}/T_0$ turbidity modes for the cases (x), (○) and (◇), respectively. (c) The relative increase $\Delta S / S_0$ in the membrane surface area calculated from the axis ratio p = c/b, where $\Delta S = S - S_0$ is the increase in the membrane area, $S_0 = 4\,\pi\,a^2$ the projected surface area at E = 0 and S the projected area in the field E. The solid lines represent the theoretical curves for membrane stretching and smoothing calculated with the membrane stretching modulus: K = 0.225 Nm^{-1}, the membrane bending rigidity $\kappa = 3.5 \cdot 10^{-20}$ J and the initial surface tension $\sigma_0 = 2.1 \cdot 10^{-4}$ N / m for the case (x); see (a). For (○): K = 0.83 Nm^{-1}, $\kappa = 1.29 \cdot 10^{-19}$ J and $\sigma_0 = 4.0 \cdot 10^{-8}$ N / m and for (◇): K = 1.2 Nm^{-1}, $\kappa = 1.71 \cdot 10^{-19}$ J and $\sigma_0 = 1.0 \cdot 10^{-8}$ N / m .

The turbidity relaxations $\Delta T^-(t)/T_0$ and $\Delta T^+(t)/T_0$ at $\lambda = 365$ nm in the vesicle suspension are opposite in sign and have different kinetics (Fig. 2 a), indicating different processes. Specifically, the negative sign of the $\Delta T^+/T_0$ relaxations indicates a decrease in the refractive index n_{lip} of membrane, caused by field-induced entrance of water into the membrane. The positive sign of $\Delta T^-/T_0$ relaxations is dominantly due to the vesicle electro-elongation in the direction of the external field vector.[27] The turbidity terms $\Delta T^-/T_0$ and $\Delta T^+/T_0$ are used for the computation of the deformation ratio p (Fig. 2 b, Fig. 3) and the relative refractive index $m = n_{lip} / n_{med}$ (Fig. 4) in the electric field E with the numerical code of Farafanov et al.[31], respectively. In the electric field, the originally spherical vesicles elongate to ellipsoids of revolution, characterized here by the semi-axis c and b, where c > b (Fig. 3).

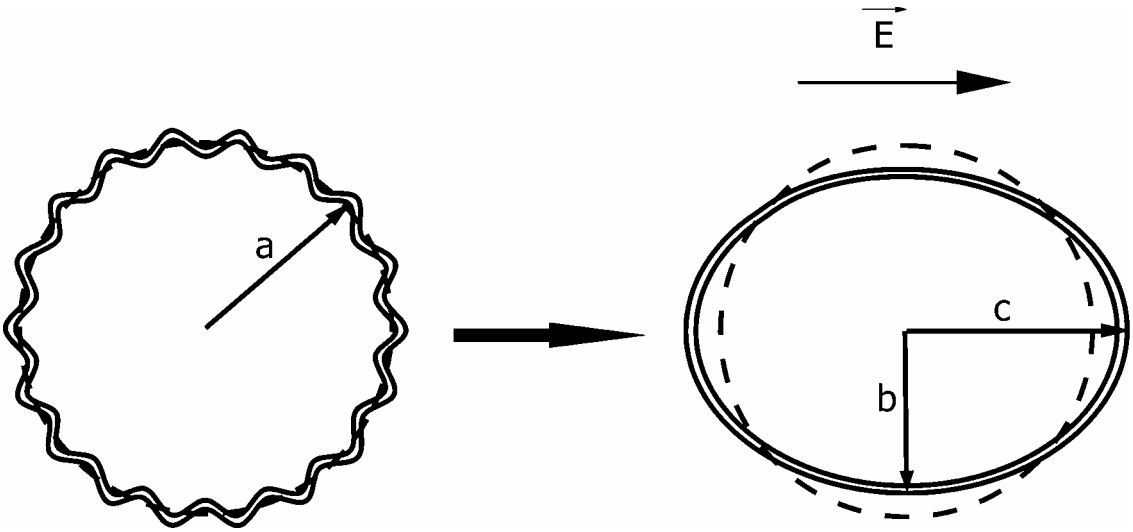

Fig. 3 Scheme for the elongation of an undulating spherical vesicle at constant volume by field-induced smoothing of the membrane undulations. $S_0 = 4\pi \cdot a^2$ refers to the dashed line representing the projected area.

The calculated deformation ratio p = c / b of the lipid vesicles increases with increasing total concentration $[D_t]$ of DNA and, as expected, with the field strength E (Fig. 2 b). At the relatively low field strength, $E = 40\ kV/cm$, the maximum stationary value $\Delta\varphi = -1.5 \cdot E \cdot a$ of the induced potential difference $\Delta\varphi$ across the membrane of the pole caps of the vesicles of the radius a = 150 nm does not exceed 0.9 V, therefore there is no measurable efflux of electrolyte from the vesicles.[32,33] Since the vesicle volume remains constant during the whole pulse length t_E = 10 µs, the relative increase $\Delta S/S_0$ in the membrane area is solely determined by the axis ratio p:[27]

$$\frac{\Delta S}{S_0} = \frac{p^{-2/3}}{2} + \frac{p^{1/3} \cdot \arcsin(\sqrt{1-p^{-2}})}{2 \cdot \sqrt{1-p^{-2}}} - 1 \qquad (4)$$

where $\Delta S = S - S_0$ is the increase in the membrane area, $S_0 = 4 \cdot \pi \cdot a^2$ the projected membrane surface area at E = 0 and S the membrane area in the field E. The membrane surface area $\Delta S(t)$ increases concomitant with the vesicle elongation ratio p. However, the time constant is different (Fig. 2 c). The relaxation of $\Delta S(t)$ for the pure lipid vesicles, without Ca^{2+} and DNA, is faster than the relaxation $\Delta S(t)$ in the presence of Ca^{2+} ions, yet the amplitude ΔS is smaller. The more DNA is adsorbed to the vesicle surface as a ternary DNA/Ca/lipid complex, the larger is the amplitude ΔS.

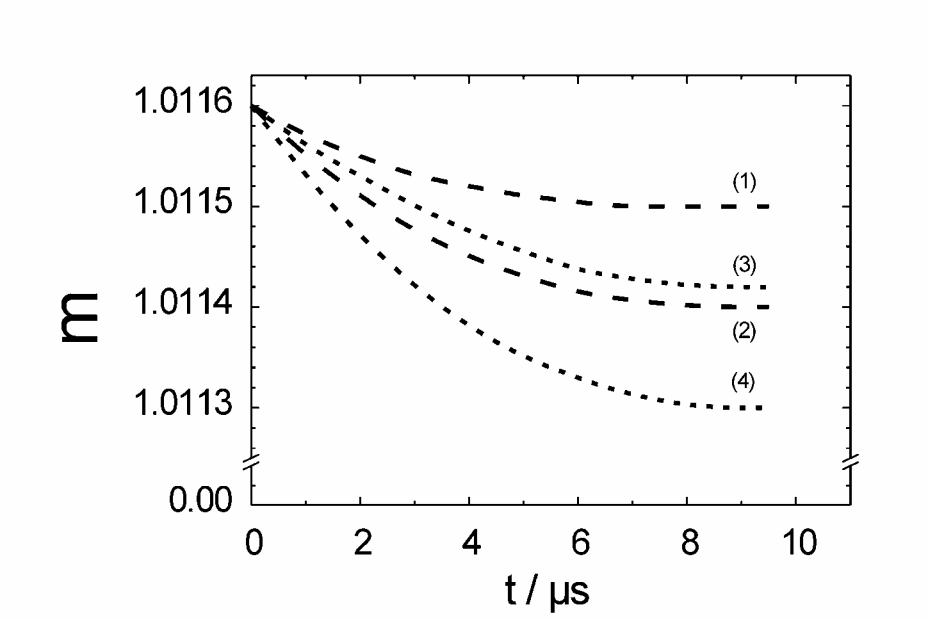

Fig. 4 The relative refractive index $m = n_{lip} / n_{med}$ of the vesicle membrane as a function of time t at the two field strengths E / (kV/cm) = 30 (1, 2) and 40 (3, 4) and for the two total DNA concentrations $[D_t]$ / µM (bp) = 0 (1, 3) and 142 (2, 4), respectively, calculated from the relaxation modes $\Delta T^{-}/T_0$ and $\Delta T^{+}/T_0$. Here n_{lip} and n_{med} are the refractive indices of the lipids and of the medium (buffer), respectively. At E = 0, the initial values of the indices are: $n_{lip}(0) = 1.3639$, $n_{med}(0) = 1.3483$ and $m(0) = 1.0116$. Other experimental conditions as in the legend to Fig.1.

Kinetic Analysis of Membrane Area Increase. Primarily, the increase $\Delta S(t)$ in the membrane surface area (Fig. 3) reflects membrane stretching (MS, $\Delta S_{MS}(t)$) and smoothing of membrane undulations (SU, $\Delta S_{SU}(t)$), respectively.[26] The total increase is the sum $\Delta S(t) = \Delta S_{MS}(t) + \Delta S_{SU}(t)$. The term $\Delta S_{MS} = \Delta S_{MS}^{\ell} + \Delta S_{MS}^{g}$ refers to both the components $T_{\ell} = (3/8) \cdot (E \cdot a)^2 \cdot C_m$ and $T_g = (3/80) \cdot a \cdot \varepsilon_0 \varepsilon_w \cdot E^2$ of the local and global Maxwell stress tensor, respectively. The individual terms are:[27]

$$\frac{\Delta S^{\ell}_{MS}(t)}{S_0} = \frac{T_{\ell}}{K} \cdot \left(1 - \exp(-t/\tau_{pol})\right)^2 \quad , \tag{5}$$

$$\frac{\Delta S^{g}_{MS}(t)}{S_0} = \frac{T_g}{K} \cdot \left(1 - \exp(-t/\tau_{pol})\right) \quad , \tag{6}$$

respectively, where K is the stretching modulus of the lipid membrane, $\tau_{pol} \approx a \cdot C_m \cdot (\lambda_{in}^{-1} + \lambda_{ex}^{-1}/2) = 0.56$ μs the time constant of the ionic membrane polarization and $C_m = 0.5$ μFcm^{-2} the specific membrane capacitance.[34] The conductivities λ_{in} and λ_{ex} refer to the intra- and extravesicular solution, respectively; here $\lambda_{in} = \lambda_{ex} = 2.0$ mS/m, ε_0 is the vacuum permittivity and $\varepsilon_W \approx 80$ the dielectric constant of water at T = 293 K. The smoothing of membrane undulations is given by[26]

$$\frac{\Delta S_{SU}(t)}{S_0} = L^{-1} \cdot \ln\left(1 + \frac{T_g}{(\pi \cdot \kappa / 4 \cdot a^2) + \sigma_0}\right) \cdot \cdot \left(1 - \frac{\tau_{SU} \cdot \exp(-t/\tau_{SU}) - \tau_{pol} \cdot \exp(-t/\tau_{pol})}{\tau_{SU} - \tau_{pol}}\right) \tag{7}$$

where κ is the bending rigidity of the lipid membrane, $L = 8\pi \cdot \kappa / (k_B T)$ is the dimensionless smoothing constant, σ_0 the initial lateral tension of the membrane. The characteristic time τ_{SU} of membrane smoothing is given by[26]:

$$\tau_{SU} \approx \frac{3\eta \cdot a^3}{\frac{48 \cdot \kappa}{5} + \frac{3}{2}\sigma_o \cdot a^2 \cdot \left(1 + \frac{K}{\sigma_o + K \cdot L^{-1}}\right)} \tag{8}$$

where η is the solution viscosity. The eqns. (5-8) of the surface relaxation yield the adequate description of $\Delta S(t)/S_0$ (Fig. 2 c) and provide the values of the elastic constants κ and K as fitting parameters (Fig. 5).

Discussion

Bending rigidity of curved lipid bilayers is decreased by DNA adsorption. As seen in Fig. 5, the vesicle membrane bending rigidity κ and the compressibility modulus K decrease with increasing total concentration of the DNA fragments [D_t]. For instance, at E = 30 kV/cm and [Ca_t] = 0.25 mM, the membrane-bound DNA in the concentration range $0 \le [D_b]/\mu M(bp) \le 40$, i.e., $0 \le N_b \le 118$ DNA fragments per one vesicle, leads to a decrease of κ in the range $17 \ge \kappa/(10^{-20} J) \ge 13$ and of K in the range $1.2 \ge K/(N/m) \ge 0.83$, respectively.

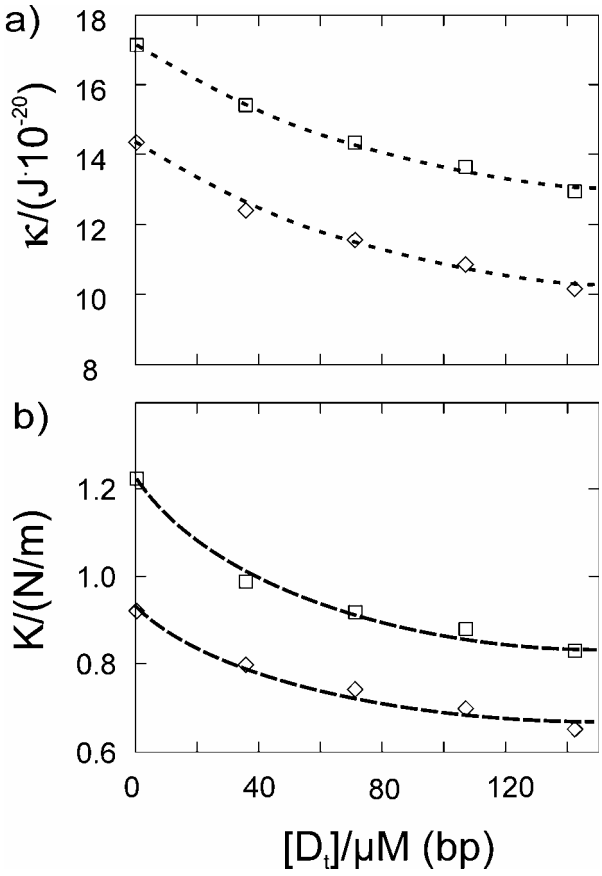

Fig. 5 The bending rigidity κ (a) and the stretching modulus K (b) of the lipid membrane of the vesicles at $[Ca_t]$ = 0.25 mM as a function of the total DNA concentration $[D_t]$ at the two field strengths: E / (kV/cm) = 30 (□) and 40 (◇), respectively, calculated from the $\Delta S(t) / S_0$ - relaxations in Fig. 2 (c). Other experimental conditions as in the legend to Fig. 1.

The decrease of κ and K with increasing $[D_b]$ is consistent with the well known fact that adsorbed polymers *always* reduce the membrane stiffness, hence here κ and K are reduced by the adsorption of DNA-polymers.[35,36] In the presence of DNA the membrane is thus more flexible and the vesicle can be easier elongated than without adsorbed DNA. Interestingly, the relative refractive index $m = n_{lip} / n_{med}$ of the vesicle membrane in the electric field decreases with increasing DNA concentration (Fig. 4), concomitant with the decrease in OD_0 at E = 0 (Fig. 1 b). The decrease in m in the electric field is consistent with a softening of the membrane due to entrance of water molecules into the head group region of the membrane lipids.[37]

Ca^{2+} adsorption increases the bending rigidity of curved lipid bilayers. The adsorption of Ca^{2+}-ions on the surfaces of the two membrane leaflets of the bilayer membrane dramatically increases the values of κ and K. For example, at $[Ca_t] = [D_t] = 0$ and

at E = 30 kV/cm, the compression modulus K = 0.225 Nm^{-1} and the membrane bending rigidity $\kappa = 3.5 \cdot 10^{-20}$ J are relatively small and compare well with reference values.[38] In the presence of $[Ca_t]$ = 0.25 mM and at $[D_t] = 0$, the elastic parameters dramatically increase up to K = 1.2 Nm^{-1} and $\kappa = 1.71 \cdot 10^{-19}$ J. The rigidifying effect of the Ca^{2+}-adsorption on the lipid membrane can be rationalized by the 'electrostatic bridges', i.e., localized complexes between several negatively charged PS-head groups and Ca^{2+}-ions on the membrane surface, concomitant with the increase in the hydrocarbon chain order of membrane lipids.[39,40] Differently to K and κ, the initial membrane surface tension $\sigma_0 = 2.1 \cdot 10^{-4}$ N/m at $[Ca_t] = [D_t] = 0$ decreases to $\sigma_0 = 1.0 \cdot 10^{-8}$ N/m for $[Ca_t]$ = 0.25 mM and $[D_t] = 0$. The decrease of σ_0 in the presence of Ca^{2+}-ions can be rationalized by the reduction of the electrostatic repulsions between the negatively charged PS-head groups of lipids by the adsorbed Ca^{2+} -ions.

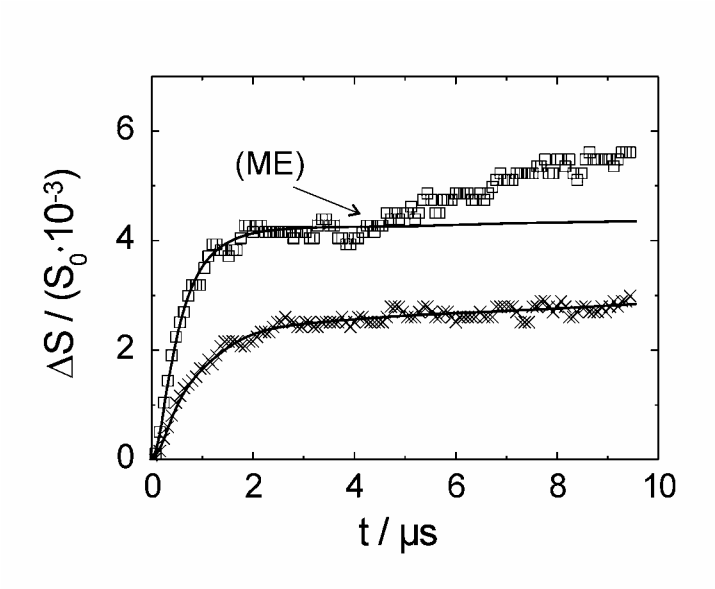

Fig. 6 The relaxations of the relative increase $\Delta S / S_0$ in the membrane surface area for the two field strengths E / (kV/cm) = 30 (x) and 40 (□) at $[D_t] = [Ca_t] = 0$. Other experimental conditions as in the legend to Fig. 1. The solid lines represent the membrane stretching and smoothing of undulations with the overall time constant τ_I = 0.7 μs. At E = 40 kV/cm, the new (electroporation) phase $\Delta S_{II}(t) / S_0$ starts at about 4 μs after the start of pulse (indicated by "ME" and the arrow). This second relaxation phase reflects the formation of membrane pores. The time constant is estimated τ_{II} = 3.5 μs and the amplitude is $\Delta S_{II} \approx 0.25 \cdot \Delta S$, i.e., about 25% of the total increase in the $\Delta S / S_0$.

The dependence of K and κ on $[Ca_t]$ can hardly be justified by a Ca^{2+}-induced gel-liquid crystalline phase transition in the vesicle membrane,[41] because the transition

temperature of the PS:2POPC lipid mixture is lower than the working temperature 293 K (20°C).[42]

The electric field decreases the bending rigidity of curved lipid bilayers. The data in Fig. 5 suggest that κ and K decrease with increasing field strength E. The decrease in κ and K with increasing E is hardly due to membrane electroporation (ME).[2] In vesicles, the fraction of membrane pores usually does not exceed 1-2% of the total membrane surface area S_0.[27] As seen in Fig. 6, at E = 40 kV/cm, the formation of membrane pores only starts about 4 μs after the field application, as a delayed new kinetic phase. At E = 30 kV/cm, the appearance of the electropores is still not noticeable. Therefore, all the calculations of the κ and K parameters from the increase ΔS in the projected area are not affected by ME. On the same line, analogous to the field-dependent decrease in the relative refractive index m (Fig. 4), the decrease in κ and K at larger fields (E = 40 kV/cm) is caused by the loss of the membrane stiffness due to the field-driven entrance of water into the surface of the outer layers of the vesicle pole cap regions.

Conclusion

In summary, the electrooptic relaxation data of PS:2POPC lipid vesicles of radius a = 150 ± 45 nm indicate that the bending rigidity κ and the compression modulus K of curved lipid bilayers decrease by DNA adsorption. The decrease in κ and K is rationalized by the field-induced entrance of water into the outer layer of the membrane bilayer. Differently to DNA adsorption and to the presence of fields, the adsorption of Ca^{2+} -ions to the negatively charged lipids of the membrane causes a dramatic increase in the membrane stiffness. Membrane electroporation is only 'visible' at the field strengths E ≥ 40 kV/cm, characterized by a delay time of ≤ 4 μs.

Acknowledgment. We gratefully thank the Deutsche Forschungsgemeinschaft for financial support, grant Ne 227/9-3, /9-4 to E. Neumann.

References

[1] E. Neumann, in *Electroporation and Electrofusion in Cell Biology*, ed. E. Neumann, A.E. Sowers and C. Jordan, Plenum Press, New York, 1989, p. 61-82.

[2] E. Neumann, M. Schaefer-Ridder, Y. Wang and P.H. Hofschneider, *EMBO J.*, 1982, **1**, 841-845.

[3] L.M. Mir, M.F. Bureau, J. Gehl, R. Rangara, D. Rouy, J.-M. Caillaud, P. Delaere, D. Branellec, B. Schwartz and D. Scherman, *Proc. Natl. Acad. Sci. USA*, 1999, **96**, 4262-4267.

[4] L.M. Mir, S. Orlowski, J. Belehradek Jr., J. Teissie, M.P. Rols, G. Sersa, D. Miklavcic, R. Gilbert and R. Heller, *Bioelectrochem. Bioenerg*., 1995, **38**, 203-207.

[5] S. Satkauskas, M.F. Bureau, M. Puc, A. Mahfoudi, D. Scherman, D. Miklavcic and L.M. Mir, *Mol. Ther.*, 2002, **5**, 133-140.

[6] R. Elez, A. Piiper, B. Kronenberger, M. Kock, M. Brendel, E. Hermann, U. Pliquett, E. Neumann and S. Zeuzem, *Oncogene*, 2003, **22**, 69-80.

[7] E. Neumann, K. Toensing, S. Kakorin, P. Budde and J. Frey, *Biophys. J.*, 1998, **74**, 98-108.

[8] K. Tönsing, S. Kakorin, E. Neumann, S. Liemann and R. Huber, *Eur. Biophys. J.*, 1997, **26**, 307-318.

[9] E. Neumann and S. Kakorin, *Radiol. Oncol*, 1998, **32**, 7-17.

[10] E. Sackmann, in *Handbook of Biological Physics: Structure and Dynamics of Membrane*, ed. R. Lipowsky and E. Sackmann, Elsevier Science B.V., Amsterdam, 1995, p. 213.

[11] R. Lipowsky and H.-G. Doebereiner, *Europhys. Lett*., 1998, **43**, 219-225.

[12] R. Lipowsky, *Europhys. Lett*., 1995, **30**, 197-202.

[13] J. Simon, M. Kuehner, H. Ringsdorf and E. Sackmann, *Chem. Phys. Lip*., 1995, **76**, 241-258.

[14] H.-G. Doebereiner, O. Selchow and R. Lipowsky, *Eur. Biophys. J.*, 1999, **28**, 174-178.

[15] S. Kakorin and E. Neumann, *Ber. Bunsenges. Phys. Chem.*, 1998, **102**, 670-675.

[16] E. Neumann, S. Kakorin, I. Tsoneva, B. Nikolova and T. Tomov, *Biophys. J*., 1996, **71**, 868-877.

[17] D. Hirsch-Lerner and Y. Barenholz, *Biochim. Biophys. Acta*, 1998, **1370**, 17-30.

[18] B. J. Battersby, R. Grimm, S. Huebner and G. Cevc, *Biochim. Biophys. Acta*, 1998, **1372**, 379-383.

[19] Y. Xu and F. C. Szoka Jr., *Biochem*., 1996, **35**, 5616-5623.

[20] S.J. Eastman, C. Siegel, J. Tousignant, A.E. Smith, S.H. Cheng and R.K. Scheule, *Biochim. Biophys. Acta*, 1997, **1325**, 41-62.

[21] A.M.I. Lam and P.R. Cullis, *Biochim. Biophys. Acta*, 2000, **1463**, 279-290.

[22] C. Fleck, R.R. Netz and H.H. von Grünberg, *Biophys. J.*, 2002, **82**, 76-92.

[23] S. Huebner, B.J. Battersby, R. Grimm and G. Cevc, *Biophys. J.*, 1999, **76**, 3158-3166.

[24] S. May, D. Harries and A. Ben-Shaul, *Biophys. J.*, 2000, **78**, 1681-1697.

[25] J. Rosenberg, N. Duezguenes and C. Kayalar, *Biochim. Biophys. Acta*, 1983, **735**, 173- 180.

[26] S. Kakorin, Th. Liese and E. Neumann, *J. Phys. Chem. B*, 2003, **107**, 10243-10251.

[27] T. Griese, S. Kakorin and E. Neumann, *Phys. Chem. Chem. Phys.* 2002, **4**, 1217-1227.

[28] S. Kakorin and E. Neumann, *Ber. Bunsenges. Phys. Chem.* 1996, **100**, 721-722.

[29] A. Rezvin and E. Neumann, *Phys. Chem.,* 1974, **2**, 144-150.

[30] C. S. Chong and K. Colbow, *Biochim. Biophys. Acta*, 1976, **436**, 260-282.

[31] V. G. Farafanov, N. V. Voshchinnikov and V.V. Somsikov, *Appl. Opt.*, 1996, **35**, 5412-5426.

[32] S. Kakorin, and E. Neumann, *Ber. Bunsenges. Phys. Chem.* 1998, **102**, 670-675.

[33] S. Kakorin, E. Redeker, and E. Neumann, *Eur. Biophys. J.*, 1998, **27**, 43-53.

[34] H.P. Schwan, *Adv. Biol. Med. Phys*., 1957, **5**, 147-209.

[35] F. Clement, and J.-F. Joanny, *J. Phys. II France*, 1997, **7**, 973-980.

[36] K.T. Skau, and E.M. Blokhuis, *Eur. Phys. J. E*, 2002, **7**, 13-22.

[37] E. Neumann, S. Kakorin and K. Toensing, *Faraday Discuss*., 1998, **111**, 111-125.

[38] U. Seifert and R. Lipowsky, in *Handbook of Biological Physics: Structure and Dynamics of Membrane*, ed. R. Lipowsky and E. Sackmann, Elsevier Science B.V., Amsterdam, 1995, p. 403.

[39] D. Huster, K. Arnold and K. Gawrisch, *Biophys. J.*, 2000, **78**, 3011-3018.

[40] D. Huster, A.J. Jin, K. Arnold and K. Gawrisch, *Biophys. J.*, 1997, **73**, 855-864.

[41] M. Thürk and D. Pörschke, *Biochim. Biophys. Acta*, 1991, **1067**, 153-158.

[42] M. G. Cevc and J. Seddon, in *Phospolipid Handbook* ed. G. Cevc, Marcel Dekker, Inc., New York, 1993, p. 351-402.

Glossary

a	vesicle radius
$[Ca_t]$, $[D_t]$	total concentration of Ca^{2+} and DNA, respectively
E	external applied field
$[D_b]$	concentration of bound DNA in the pellet
κ, K	bending rigidity and stretching modulus of the membrane, respectively
$[L_t]$	total lipid concentration
$m = n_{lip} / n_{med}$	relative refractive index of the vesicle membrane
ME	membrane electroporation
n_{lip}, n_{med}	refractive index of the lipid membrane and medium, respectively
OD_0	initial optical density at the wavelength λ = 365 nm
p	axis ratio of the elongated vesicle
PS	phosphatidylserine
POPC	palmitoyl-oleoyl-phosphatidylcholine
σ_0	initial lateral tension of the membrane
t_E	pulse duration
VET	vesicle extrusion technique

Danksagung

Die vorliegende Dissertation wurde in der Zeit von Februar 2000 bis April 2005 am Lehrstuhl für Physikalische und Biophysikalische Chemie, Fakultät für Chemie, Universität Bielefeld unter der Leitung von Herrn Prof. Dr. E. Neumann durchgeführt.

Herrn Prof. Dr. E. Neumann danke ich herzlich für die Themenstellung, zahlreiche wissenschaftliche Diskussionen und die Unterstützung in allen täglichen Problemen. Weiterhin möchte ich mich bei Prof. Dr. E. Neumann für die Möglichkeit der Teilnahme an wissenschaftlichen Tagungen und Kongressen bedanken.

Ein besonders herzlicher Dank geht an Frau Dr. Katja Tönsing für eine gute Zusammenarbeit, Einführung in der Technik der Feldsprungmessverfahren, Bereitschaft für Diskussionen, Verbesserung und Korrekturlesen des Manuskriptes und Hilfsbereitschaft in allen täglichen Problemen mit Rat und Tat.

Herrn Dr. Sergej Kakorin möchte ich für die Beiträge zur Theorie, die gute Zusammenarbeit und für zahlreiche Diskussionen zur Auswertung der experimentellen Daten danken.

Weiterhin möchte ich mich ganz herzlich bei allen meinen Arbeitskollegen bedanken, ins besondere bei den technischen Assistenten, für die gute Arbeitsatmosphäre und Freundlichkeit.

Nicht zuletzt danke ich meiner Familie und meinen Freunden, die mich in diesen Jahren immer sehr unterstützt und mir Mut gegeben haben.

Abschließend gilt mein Dank der Deutschen Forschungsgemeinschaft (DFG) für die finanzielle Unterstützung des Projektes Ne 227/9-3, /9-4 an E. Neumann.